Advances in the measurement and computation of thermal phonon transport properties

2015 J. Phys.: Condens. Matter 27 053202

(http://iopscience.iop.org/0953-8984/27/5/053202)

IOP Publishing Journal of Physics: Condensed Matter
J. Phys.: Condens. Matter **27** (2015) 053202 (21pp) doi:10.1088/0953-8984/27/5/053202

Topical Review

Advances in the measurement and computation of thermal phonon transport properties

A J Minnich

Division of Engineering and Applied Science, California Institute of Technology, Pasadena, CA 91125, USA

E-mail: aminnich@caltech.edu

Received 2 May 2014, revised 28 November 2014
Accepted for publication 4 December 2014
Published 21 January 2015

Abstract

Heat conduction by phonons is a ubiquitous process that incorporates a wide range of physics and plays an essential role in applications ranging from space power generation to LED lighting. Heat conduction has been studied for over two hundred years, yet many of the microscopic details have remained unknown in most crystalline solids, including which phonon–phonon interactions are primarily responsible for thermal resistance and how heat is distributed among the broad thermal spectrum. This lack of knowledge was the result of limitations on the available tools to study heat conduction. However, recent advances in both computation and experiment are enabling an unprecedented microscopic view of thermal transport by phonons in both bulk and nanostructured crystals, from the level of atomic bonding to mesoscopic transport in complex devices. In this topical review, we examine these techniques and the microscopic insights gained into the science and engineering of heat conduction.

Keywords: thermal transport, heat conduction, phonons, ballistic transport, thermoelectrics

(Some figures may appear in colour only in the online journal)

1. Introduction

Heat conduction by phonons in solids is a fundamental process that incorporates a variety of fascinating physics in addition to playing a central role in numerous applications. At the macroscale, heat conduction is accurately described by diffusion theory based on Fourier's law, which states that the heat flux is linearly related to a temperature gradient by a material property, the thermal conductivity. However, accessible length and time scales have dramatically decreased over the past 30 years, and when these scales are comparable to phonon mean free paths (MFPs) and relaxation times, respectively, macroscopic theories do not provide an accurate picture of the transport [1, 2]. For example, Fourier's law substantially underpredicts, by tens of K, the temperature rises of localized hotspots at the junctions of transistors [3, 4], an error that affects reliability and performance predictions for electronic devices. The lifetimes of LEDs for domestic lighting as well as the performance of high power transistors is limited by near-junction thermal resistances due to defects and interfaces near the active region of these devices [5–7]. On the other hand, new nanostructured materials have been created with substantially reduced thermal conductivities compared to those of the bulk material, and some of these materials are under development as thermoelectric materials for applications in waste heat recovery [8–13]. Accurately describing thermal transport in such applications requires a microscopic perspective of phonon transport in solids, particularly knowledge of the phonon dispersion and intrinsic and extrinsic scattering mechanisms over the broad blackbody phonon spectrum.

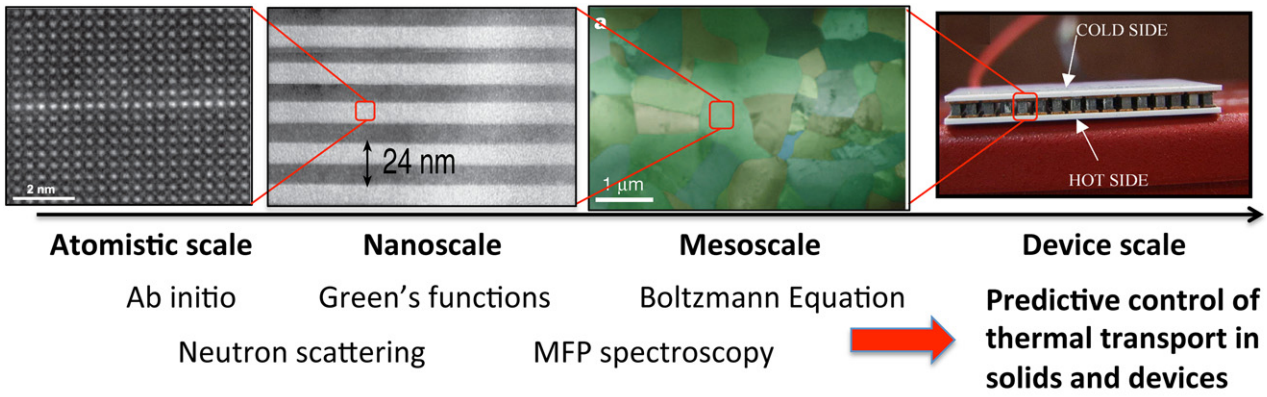

Figure 1. Schematic overview of the new tools to study heat conduction that are enabling a microscopic understanding of the origin of thermal conductivity, ranging from the atomistic scale which considers the nature of atomic bonding and phonon–phonon interactions all the way to the mesoscale and device scale. Images adapted from [8, 26–28].

The modern study of thermal conductivity began with Debye in 1914, who first attributed heat conduction to delocalized lattice waves and was able to explain the $1/T$ temperature dependence of thermal conductivity at sufficiently high temperatures [14]. Peierls then introduced the phonon Boltzmann equation and identified the two anharmonic interactions, normal and Umklapp processes, that return phonons to thermal equilibrium [15]. Subsequently, in the 1940s and 50s, approximate expressions for relaxation times due to different scattering mechanisms such as anharmonicity, point defects, and dislocations were derived by Pomeranchuk, Klemens, and Herring, among others [16–18]. In the early 1960s, Callaway, Holland, and others introduced models of thermal conductivity that could reasonably explain the temperature dependent thermal conductivity of pure crystals and alloys [19–21]. In fact, these models are still in frequent use today to study thermal transport in a wide range of materials. Microscopic phonon transport properties can be obtained by adjusting model parameters to fit macroscopic thermal conductivity data.

While this approach does yield useful insight, it has substantial limitations. First, the approach is not predictive because the fitting parameters must be determined using experimental data before any conclusions can be drawn. Second, the extracted MFPs strongly depend on assumptions made in the fitting and thus are difficult to determine unambiguously. For example, assuming a solid has a Debye dispersion leads to the contribution of high frequency phonons being substantially overpredicted because actual zone-edge phonons have a much smaller group velocity than the sound velocity [22–25]. Further, if multiple scattering mechanisms with different temperature dependencies are present, as in complex thermoelectric materials, separating the various mechanisms is challenging. These ambiguities fundamentally occur because thermal conductivity represents an average over all phonon modes that results in a loss of the microscopic details of thermal transport. As a result, basic questions about the transport properties of thermal phonons remain unanswered, including the values of phonon propagation lengths in simple crystals like Si and diamond, which phonons transmit heat across crystalline interfaces, and many others.

Fortunately, a number of advances in both computation and experiment are providing these microscopic details from the atomistic level all the way to the device scale, as illustrated in figure 1. Computational *ab initio* methods now allow predictive, parameter-free studies of the role of atomic bonding and phonon–phonon interactions in setting thermal conductivity; atomistic Green's functions enable calculations of phonon scattering from nanostructures and transmission through interfaces; and new, efficient Monte Carlo algorithms are able to simulate transport through complex mesoscale structures. Through these parameter-free approaches, for the first time computation is providing predictions to be verified by experiment rather than the traditional reverse path. In experiment, methods such as inelastic neutron scattering, as well as a new experimental technique called mean free path spectroscopy, are providing the first direct measurements of the transport properties resolved across the thermal phonon spectrum. In this topical review, we provide an overview of these techniques and their impact on the science and engineering of thermal conductivity in both bulk and nanostructured materials.

We note that a number of reviews in the general area of nanoscale thermal transport have recently been published [1, 24, 29–31]. In this review, we focus specifically on advances in computation and experiment for studying thermal phonon transport. The reader is referred to other reviews for a broader view of the nanoscale thermal transport field.

2. Thermal transport by phonons

From the most fundamental perspective, phonons are waves, and therefore accurately describing thermal transport by phonons requires a formalism that accounts for this wave nature. Indeed, describing phonon transmission across an interface or scattering from an atomic point defect requires an approach such as atomistic Green's functions, described in section 3.2, that rigorously includes wave effects on a discrete atomic lattice. However, considering that phonon wavelengths are typically only a few nanometers at room temperature, in many practical situations these atomistic scale wave effects

can be incorporated as scattering mechanisms into a particle-based transport formalism that itself does not explicitly account for wave effects. Though recent experiments suggest that the wave nature of phonons can play a role in thermal transport in superlattices [26, 27], for most situations the particle-based picture is an accurate representation of the transport in both bulk and nanostructured crystals.

In the particle treatment, thermal phonon transport is governed by the Boltzmann transport equation (BTE), which is an equation governing a scalar distribution function $\Psi_\lambda(\mathbf{r}, t)$ that describes the probability of finding a phonon in time, real space, and phase space. This equation has a long history and describes diverse phenomena ranging from photon transport through scattering atmospheres [32] to neutron transport in nuclear reactors [33]. The equation was introduced for phonons in solids including the complete anharmonic collision term by Peierls in 1929 [15], and solutions of the BTE with simpler collision terms were obtained using mathematical techniques from neutron transport theory by Engleman as early as 1958 [34]. The BTE is only valid at length scales larger than phonon wavelengths but in this range remains valid for arbitrary values of the phonon MFPs, from the diffusive to the ballistic limits. In contrast, macroscopic heat diffusion theory is only valid if MFPs are much smaller than the characteristic length scales of thermal gradients.

The phonon BTE is given by: [35, 36]

$$\frac{\partial \Psi_\lambda}{\partial t} + \mathbf{v}_\lambda \cdot \nabla_\mathbf{r} \Psi_\lambda = \left(\frac{\partial \Psi_\lambda}{\partial t}\right)_c \tag{1}$$

where Ψ_λ is the desired distribution function, $\mathbf{v}_\lambda$ is the group velocity, $\mathbf{r}$ is the spatial coordinate, t is time, and λ denotes a particular phonon mode of wavevector $\mathbf{q}$ and polarization j. The left-hand side of the equation describes the change in phonon population in a particular region of phase space due to advection induced by spatial gradients and temporal variations, while the right-hand side represents the collision term that describes the rate at which phonons enter and leave the phase space region due to interactions with other phonons and the environment. The principal difficulty of the BTE is due to the collision term, and the methods to solve the equation vary greatly depending on the chosen form of the collision integral.

In the thermal sciences, equation (1) is typically solved under one of two approximations: a linearized collision term that accounts for inelastic 3-phonon coupling, and the single-mode relaxation time approximation (RTA) that neglects inelastic processes but yields a simpler collision integral suitable for computing transport dynamics.

2.1. 3-phonon collision integral

The BTE with the 3-phonon collision integral is most often specified under the assumption of a uniform, one-dimensional temperature gradient and a linearized collision integral such that an expression for thermal conductivity can be obtained and evaluated. Under these assumptions, the BTE is given by: [35, 36]

$$\begin{aligned} v_{\beta\lambda}\frac{\partial T}{\partial x_\beta}\frac{\partial n^0_\lambda}{\partial T} = &\sum_{\lambda',\lambda''}\Bigg[W^+_{\lambda\lambda'\lambda''}(\Psi_{\lambda''} - \Psi_{\lambda'} - \Psi_\lambda) \\ &+\frac{1}{2}W^-_{\lambda\lambda'\lambda''}(\Psi_{\lambda''} + \Psi_{\lambda'} - \Psi_\lambda)\Bigg] \\ &+\sum_{\lambda'} W^{\text{elastic}}_{\lambda,\lambda'}(\Psi_{\lambda'} - \Psi_\lambda) - n^0_\lambda(n^0_\lambda + 1)\Psi_\lambda\frac{1}{\tau_{\text{ext}}} \end{aligned} \tag{2}$$

where n^0_λ is the Bose–Einstein distribution, T is the absolute temperature, $W^\pm_{\lambda\lambda'\lambda''}$ are the 3-phonon scattering matrices, $v_{\beta\lambda}$ is the group velocity along direction x_β, $W^{\text{elastic}}_{\lambda,\lambda'}$ is the scattering matrix for elastic processes such as point defect scattering, and τ_{ext} is the relaxation time for extrinsic processes such as boundary scattering. Note that this form of the collision integral considers only 3-phonon processes, neglecting 4-phonon and higher order phonon processes. This simplification is justified in most cases because higher order phonon processes are much less likely to occur than 3-phonon processes and thus contribute little to thermal resistance under typical conditions [37].

Once this equation has been solved for Ψ_λ, the thermal conductivity tensor of a crystal $\kappa_{\alpha\beta}$ then follows as:

$$\kappa_{\alpha\beta} = \frac{1}{V}\sum_\lambda \hbar\omega v_{\alpha\lambda} n^0_\lambda(n^0_\lambda + 1)\left(\frac{-\Psi_\lambda}{\partial T/\partial x_\beta}\right) \tag{3}$$

where V is the volume of the crystal, ω is the phonon frequency, and $v_{\alpha\lambda}$ is the velocity in the x_α direction.

This formalism requires as inputs the phonon dispersion relation, which describes the phonon frequency ω_λ for different wavevectors $\mathbf{q}$ and polarizations j throughout the Brillouin zone, as well as considerable detail for the scattering mechanisms such as the 3-phonon scattering matrices. Historically, the challenge for thermal conductivity studies was that none of these quantities was available. Phonon dispersion calculations for crystals from first-principles have only become possible within the past 30 years with increasing availability of quantum mechanics computational packages and significant computing power. Phonon dispersions can be measured, as they have been for decades using inelastic neutron scattering as described in section 4.1, but experimental restrictions limited the measurements to high symmetry directions rather than the full Brillouin zone information required for thermal conductivity. As a result, early thermal conductivity studies used the linear isotropic Debye model or isotropic piecewise linear models that are often poor approximations for the actual dispersions [19, 20].

However, this problem is minor compared to the challenge of computing phonon–phonon interactions with the 3-phonon scattering matrices $W^\pm_{\lambda\lambda'\lambda''}$ as well as identifying the scattering rates for the extrinsic scattering mechanisms. The 3-phonon scattering matrices require knowledge of the cubic force constants that describe the anharmonic component of the interatomic potential, an extremely challenging calculation. Unlike the phonon dispersions, these scattering matrices are not directly measurable. Further, exact expressions for extrinsic scattering rates are available only for the simplest

cases such as for an atomic point defect [38], and approximate expressions for the scattering rates due to extended structures can only be obtained after significant simplifications that introduce fitting parameters [18, 35]. The result is that significant ambiguity remained in the precise effects of these structures on thermal phonons.

2.2. Relaxation time approximation

Due to the lack of knowledge of the 3-phonon scattering matrices, equation (2) in its full form has only been considered in recent years, as we will describe in section 3.1. Historically, the BTE was instead solved under the RTA in which the terms $\Psi_{\lambda'}$ and $\Psi_{\lambda''}$ in the collision integral are set to zero, allowing the BTE to be reduced to the following form: [28, 35, 36]

$$\frac{\partial \Psi_\lambda}{\partial t} + \mathbf{v}_\lambda \cdot \nabla \Psi_\lambda = -\frac{\Psi_\lambda - \Psi_\lambda^0(T_\mathrm{p}(\mathbf{r},t))}{\tau_\lambda} \tag{4}$$

Here τ_λ is the total relaxation time for a phonon mode and $\Psi_\lambda^0(T_\mathrm{p}(\mathbf{r},t))$ is the local equilibrium distribution that represents the distribution to which phonons relax as a function of space and time. The total relaxation time is related to the relaxation times of the individual mechanisms by Mathiessen's rule, $\tau_\lambda^{-1} = \tau_{\lambda,\mathrm{p-p}}^{-1} + \sum_i \tau_{\lambda,\mathrm{ext},i}^{-1}$, where $\tau_{\lambda,\mathrm{p-p}}$ is the relaxation time for phonon–phonon scattering [35]. Combining the relaxation times in this way assumes that the scattering mechanisms are independent of each other.

To close this form of the BTE a relationship between Ψ_λ and Ψ_λ^0 is required, which can be obtained by enforcing energy conservation. Consider multiplying equation (4) by $\hbar\omega$ and summing over all phonon modes. The resulting equation will be:

$$\frac{\partial U(\mathbf{r},t)}{\partial t} + \nabla \cdot \mathbf{q}(\mathbf{r},t) = 0 \tag{5}$$

where $U(\mathbf{r},t)$ is the local energy density and $\mathbf{q}(\mathbf{r},t)$ is the heat flux. This equation simply expresses energy conservation and thus requires that Ψ_λ and Ψ_λ^0 are related by the following equation:

$$\sum_\lambda \frac{\Psi_\lambda(\mathbf{r},t)}{\tau_\lambda} = \sum_\lambda \frac{\Psi_\lambda^0(T_\mathrm{p}(\mathbf{r},t))}{\tau_\lambda} \tag{6}$$

where $T_\mathrm{p}(\mathbf{r},t)$ is the local pseudo-temperature. Note that the pseudo-temperature differs from the thermodynamic temperature that describes the energy density due to the presence of the weighting factor τ_λ^{-1}. Equation (6) must be solved simultaneously with equation (4) to obtain a self-consistent solution of the BTE.

Under the assumption of a uniform temperature gradient, the thermal conductivity under the RTA can be identified from the BTE as:

$$\kappa_{\alpha\beta} = \frac{1}{V}\sum_\lambda C_\lambda v_{\alpha\lambda} v_{\beta\lambda} \tau_\lambda \tag{7}$$

where $C_\lambda = \hbar\omega \partial n_\lambda^0/\partial T$ is the mode specific heat. If the crystal is thermally isotropic, as are the majority of crystals, then the angular integrations can be carried out exactly and the equation can be further simplified as the familiar kinetic equation of thermal conductivity [28],

$$\kappa = \frac{1}{3}\int C_\omega v_\omega^2 \tau_\omega \mathrm{d}\omega = \frac{1}{3}\int C_\omega v_\omega \Lambda_\omega \mathrm{d}\omega \tag{8}$$

where $C_\omega = \hbar\omega D(\omega)\partial n_\lambda^0/\partial T$ is the frequency-dependent specific heat with $D(\omega)$ as the density of states, and Λ_ω is the MFP. Under the isotropic assumption, all the quantities in the integral only depend on phonon frequency.

This form of the BTE, which neglects inelastic processes, requires knowledge of the phonon dispersion and the same extrinsic scattering rates as before, but now the phonon–phonon interactions are described by effective relaxation times. The anharmonic scattering matrices over the full Brillouin zone are no longer required, resulting in substantial simplification. The RTA is accurate to within 10% in many common semiconductors like Si, although it fails for materials such as diamond [39]. In early works, scaling laws were derived for phonon–phonon interactions, such as $\tau_{\mathrm{p-p}}^{-1} \sim \omega^2 T$, that could be inserted into equation (4), and thus providing all the inputs required for the solution of the BTE once all fitting parameters were determined [16].

While the BTE under the RTA is much easier to solve than equation (2), it is still challenging because the BTE remains an integro-differential equation of seven variables—time, three spatial variables, and three momentum space variables. Until even 5 years ago, solving the equation numerically was tractable only by making simplifications such as neglecting the frequency-dependence of phonon properties or only considering one-dimensional thermal gradients.

These derivations highlight the principal challenge for understanding thermal transport: thermal resistance is due to the transport properties of phonons that vary widely over the entire Brillouin zone, but the observable quantities typically represent an average over all phonons, obscuring the microscopic details. For example, a measurement of thermal conductivity essentially condenses a complex set of phonon–phonon and phonon-defect interactions over the broad phonon blackbody spectrum into a single number. The computational and experimental techniques described in this review overcome this challenge by providing direct access to the transport properties of individual phonon modes, leading to significant advances in our understanding of heat conduction as described in this review.

3. Computation

Considerable progress in computational tools for thermal transport has occurred over length scales ranging from the atomistic level to the mesoscale. At the most fundamental level, quantum mechanical computational packages based on density functional theory (DFT) are now routinely used to provide the phonon dispersion and 3-phonon scattering matrices for equation (2) without any adjustable parameters. These calculations are for the first time driving experimental studies by providing parameter-free predictions such as the high thermal conductivity of the compound Boron Arsenide, rather than the historical approach of explaining experiment

with a simple theory with fitting parameters. At the other end of the length scale, new variance-reduced Monte Carlo algorithms enable the BTE under the RTA, equation (4), to be efficiently solved in domains exceeding 1 mm in size. In this section, we describe how these methods are implemented and how they have advanced our knowledge of heat conduction.

3.1. Ab initio

Ab initio calculations of thermal conductivity consist of using DFT to determine the interatomic potential of the atoms in a crystal, from which the inputs to equation (2) can be obtained as the dispersion relation and the anharmonic scattering matrices. We note that molecular dynamics can also be used to study heat conduction with the *ab initio* interatomic potential [40], but here we focus on the more commonly used BTE approach. Prior to the availability of *ab initio* interatomic potentials, atomistic calculations were based on semi-empirical potentials such as the Stillinger–Weber potential with adjustable parameters for each material. However, these potentials were designed to fit experimentally measured lattice constants and elastic constants, and thermal conductivity predictions were often in poor agreement with the actual values [41]. Further, empirical potentials have limited predictive power because the fitting parameters must be determined by fitting to experimental data. In contrast, the *ab initio* approach is able to accurately calculate the interatomic potential without any adjustable parameters or other inputs besides fundamental constants. As a result, this predictive approach is providing a new understanding of the origin of a material's thermal conductivity.

DFT has long been used to determine phonon dispersions by calculating the harmonic force constants between atoms [42–45]. Yin and Cohen reported calculations of nonlinear response coefficients such as cubic force constants at high symmetry points by taking finite differences of harmonic force constants. Subsequent work showed that the anharmonic force constants could be obtained using density functional perturbation theory (DFPT) and the $2n + 1$ theorem for certain crystals [46]. This approach was used to calculate the linewidths of high symmetry points in the Brillouin zone, enabling comparison to Raman measurements with excellent agreement [47, 48]. Deinzer *et al* first reported the calculation of linewidths over the entire Brillouin zone using DFPT [49]. Broido *et al* then extended this approach to compute the thermal conductivities of Si and Ge without any adjustable parameters using an exact iterative solution of the BTE (equation (2)) [37]. Later works used a real-space approach based on calculating forces due to systematic atomic displacements using DFT that can be applied to complicated crystal structures [50]. These methods have now been applied to a wide variety of materials with resounding success, ranging from pure and compound semiconductors [39, 51–59], isotopically impure crystals [60–64], nanowires [65], nanotubes [66, 67],materials under extreme pressure [68], half Heusler alloys [69], PbTe [70–72], Bi [73], lead chalcogenides [74], alloys [75], superlattices [76, 77], to 2D materials such as MoS_2 [78] and graphene [79, 80].

While the required calculation is formidable, the widespread availability of quantum mechanical simulation packages and large computers within the past 10 years have made the *ab initio* approach feasible for a wide variety of materials. The first step is to determine the phonon dispersion from the harmonic force constants obtained from DFPT. This procedure is valid provided the anharmonicity of the crystal is not sufficiently strong to alter the phonon modes, a good assumption for most materials but one that is violated by some materials such as PbTe as described in section 4.1. Next, the scattering matrices $W^{\pm}_{\lambda\lambda'\lambda''}$ must be calculated, which are related to the three-phonon scattering matrix elements by Fermi's golden rule. The golden rule in turn requires the cubic interatomic force constants, which are defined as the third derivative of the total energy with respect to atomic displacements. A frequently used approach to obtain the cubic force constants is to calculate the harmonic force constants using DFT as atoms in the computational cell are systematically displaced. The cubic force constants can then be calculated as the finite difference derivative of the harmonic force constants, thus providing the scattering matrices on the right-hand side of equation (2).

The next step is to solve the BTE, or equation (2). The principle difficulty is the collision term, which couples triplets of phonons together by 3-phonon scattering. Identifying all of the possible scattering processes that satisfy energy and momentum conservation requires many searches through the entire computational phase space that consists of hundreds of thousands of discrete points. Then, the BTE must be solved with all of these coupling terms. To do so, the collision term is written as a linear system of equations with Ψ_λ, the unknown distribution function, as the solution. This equation can be efficiently solved by iteration, with the zeroth order iteration being the relaxation time approximation of the BTE. After tens of iterations, depending on the material, the procedure converges and Ψ_λ is determined.

As described in section 2, once the distribution function is found the thermal conductivity can be calculated from equation (3). However, the solution of the BTE provides not only the thermal conductivity but also the contribution of every phonon to thermal conductivity over all of phase space as well as exactly which phonons couple to every other phonon. From these quantities we obtain a unique, microscopic perspective into thermal conduction in crystals. It is not an exaggeration to say that this perspective has fundamentally changed our understanding of thermal conductivity. We now highlight a small sampling of the insights gained into heat conduction.

One particularly important realization is the breadth of the thermal phonon spectrum and correspondingly, the importance of low frequency, long MFP phonons to heat conduction. Due to complications in determining the MFPs of phonons as discussed in the introduction, many works treated the phonon spectrum using average properties in a grey approximation. Because simple estimates of the average phonon MFP in Si based on kinetic theory predict a MFP of at most a few hundred nanometers, low frequency phonons with frequency less than 3–4 THz would not be expected to contribute to heat conduction due to their small heat capacity. However, this

estimation turns out to be very misleading. In fact, thermal phonons possess an extremely broad spectrum, with MFPs ranging from a few nanometers to 10 microns in Si at room temperature [56]. A calculation of the accumulated thermal conductivity contribution versus wavelength and MFP by Esfarjani *et al* [56] is shown in figure 2(*a*), demonstrating that while most thermal phonons have similar wavelengths, MFPs vary by orders of magnitude. Further, phonons with MFPs longer than 1 micron are predicted to contribute over 40% of the total thermal conductivity in silicon at room temperature, a result that is supported by experiment [81]. The prediction is also consistent with earlier MD simulations by Henry and Chen [82] and demonstrates the importance of considering the phonon MFP spectrum, rather than an average MFP, for interpreting thermal measurements in bulk and nanostructured materials.

Another insight is the importance of optical modes to heat conduction, although by an indirect route. Due to their small group velocity, the contribution of optical modes to heat conduction is typically neglected. Ward and Broido found this assumption to be a good one for bulk Si and Ge, [51] with optical modes contributing less than 10% although this contribution can be larger in nanostructures [83] and in some bulk materials such as PbTe [71]. However, while optical modes typically do not contribute to heat conduction substantially, they provide extremely important scattering channels for acoustic phonons. Removal of these optical modes from the scattering channels completely changes the temperature dependence of the relaxation times and results in a factor of three increase in the thermal conductivity in solids like diamond and Si as shown in figure 2(*b*). Optical modes thus play a key role in three-phonon scattering processes and hence the thermal conductivity of crystals. This work highlights the unique insights that *ab initio* methods can provide because experimentally removing the scattering by optical phonons in an actual Si sample is not possible.

Ab initio calculations have also been able to provide a microscopic understanding of what makes a material a good thermal conductor. The traditional criteria for high thermal conductivity, light atomic masses and stiff harmonic bonds, are well known [84]. While these macroscopic criteria are useful, the small number of high thermal conductivity crystals such as silicon and diamond is already known and new materials have not been identified in some time. Using first-principles calculations, Lindsay *et al* recently identified a new set of microscopic criteria for thermal conductors based on an analysis of the compound Boron Arsenide that offers substantially more insight into the origin of high thermal conductivity [62]. As illustrated in figure 2(*c*), these requirements include acoustic phonon bunching so that interactions among acoustic modes are restricted, a large acoustic-optical phonon energy gap so that optical phonons cannot participate in phonon–phonon scattering, and isotopically pure elements to eliminate point defect scattering. BAs appears to incorporate all of these mechanisms and thus could have a high thermal conductivity comparable to that of diamond. Efforts are now underway to synthesize single crystals of BAs, demonstrating that calculations can now drive experiments in the thermal sciences rather than the more traditional reverse path.

The *ab initio* approach can also be extended to alloys such as SiGe. A subtle aspect of alloys is that they consist of randomly placed mass defects and thus are not periodic. Attempting to calculate properties by progressively increasing the size of a DFT supercell with random masses can yield erroneous results such as the group velocity tending to zero. A method to overcome this issue is to employ the virtual crystal model with average atomic masses and force constants and incorporate mass defect scattering as an additional scattering mechanism. Garg *et al* used this approach to examine the thermal conductivity of Si–Ge alloys [75], finding that the point defect scattering mechanism dramatically increases the relative contribution of low frequency modes to heat conduction, as shown in figure 2(*d*), with the majority of the heat carried by sub-THz frequency phonons with MFPs between 200 nm and 3 microns. Unexpectedly, the authors also found that scattering of low frequency phonons is increased in alloys compared to the pure crystal due to a change in the vibrational eigenmodes of the random structure. The low thermal conductivity of alloys is thus due to two mechanisms, and the latter mechanism would have been very difficult to identify without *ab initio* calculations.

These highlights are just a few of the many results that have been provided by *ab initio* calculations. Other insights include a better understanding of normal processes [39] and the effect of superlattice periodicity on thermal conductivity [76, 77], among others. The *ab initio* approach has had a very important impact on our understanding of the origin of thermal conductivity from an atomistic perspective and is now able to provide predictions for experimental investigation. Further progress is expected as it is applied to a wider range of solids.

3.2. Atomistic Green's functions

While DFT provides the most detailed microscopic information, the approach is very computationally intensive and cannot be applied to domains larger than a few atomic unit cells. However, many structures such as grain boundaries and nanoparticles are too large for DFT yet sufficiently small that the wave nature of the phonon on the discrete atomic lattice must be considered. For these situations, the atomistic Green's functions (AGF) approach has emerged as a powerful technique to exactly calculate the interaction of phonons with extended structures assuming a harmonic lattice [85]. We note that molecular dynamics is also a useful approach that incorporates anharmonicity but is restricted to high temperatures [86–90]. Further information on the molecular dynamics method is available in another review [31].

Green's functions are widely used to solve differential equations. The phonon AGF method has its origins in nanoscale electron transport calculations, where it is known as the Non-Equilibrium Green's Function (NEGF) formalism [91, 92]. In this approach, the Schrodinger equation is solved in a specified domain between two contacts, yielding the transmission function across the domain as a function of energy. The advantage of this technique is that

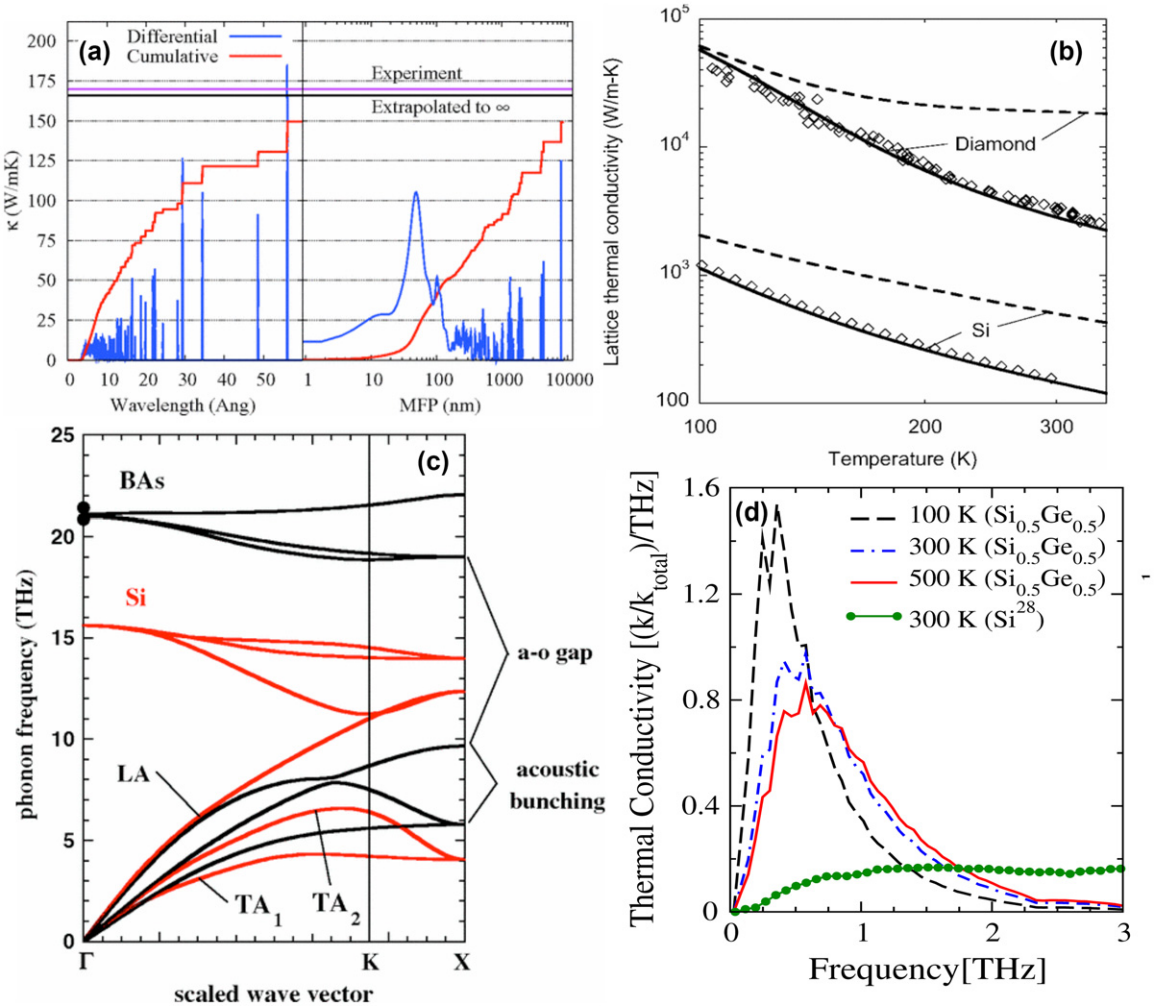

Figure 2. (*a*) Spectral thermal conductivity of silicon at 277 K versus wavelength (left) and MFP (right). Nearly half the heat is carried by phonons with MFPs exceeding 1 micron, despite their small contribution to heat capacity. Reprinted figure 6 with permission from [56]. Copyright (2011) by the American Physical Society. (*b*) Thermal conductivity of diamond and silicon versus temperature with (solid line) and without (dashed line) optical phonon scattering. Optical phonons play a key role in setting thermal conductivity by providing channels for phonon–phonon scattering, although they do not carry substantial heat in bulk materials. Reprinted figure 5 with permission from [39]. Copyright (2009) by the American Physical Society. (*c*) Microscopic mechanisms underlying the predicted high thermal conductivity of BAs, including acoustic phonon bunching and a large acoustic-optical phonon gap that inhibit phonon–phonon scattering. Reprinted figure 5 with permission from [62]. Copyright (2013) by the American Physical Society. (*d*) Spectral thermal conductivity versus phonon frequency for $Si_{0.5}Ge_{0.5}$, demonstrating that the thermal conductivity is primarily due to phonons with frequencies less than 1 THz, in contrast to bulk Si. Reprinted figure 2 with permission from [75]. Copyright (2011) by the American Physical Society.

interactions with semi-infinite contacts are exactly accounted for through self-energy terms. NEGF has been extensively used to simulate nanoscale electronic devices [93].

By making a few careful substitutions, an analogous approach can be developed for phonons [85, 94]. This adaptation was introduced by Mingo and Yang to study dielectric nanowires coated with an amorphous material [95]. Subsequently, AGF has been used to study phonon transport in a wide variety of structures, including Si/Ge interfaces [96], nanowire junctions [97], BN nanotubes [64], carbon nanotube pellets [98], solids containing nanoparticles [99], and others [27, 100–106].

Phonon AGF consists of solving for a transmission function $\Xi(\omega)$ as a function of phonon frequency ω across a center domain of interest with each side connected to semi-infinite leads. The thermal conductance σ is related to $\Xi(\omega)$ by:

$$\sigma = \frac{1}{2\pi}\int_0^{\omega_m} \hbar\omega\Xi(\omega)\frac{\partial f_0}{\partial T}\mathrm{d}\omega \tag{9}$$

where f_0 is the Bose–Einstein distribution, T is the absolute temperature, and ω_m is the maximum phonon frequency in the solid [28]. The transmission function is given by:

$$\Xi(\omega) = \mathrm{Tr}\left(\Gamma_\mathrm{L} G^\mathrm{R} \Gamma_\mathrm{R} G^\mathrm{A}\right) \tag{10}$$

where Tr denotes trace, Γ_L and Γ_R describe the phonon current entering and leaving the leads, respectively, and G^R and G^A are the retarded and advanced Green's functions, respectively [85]. These quantities can be related to the harmonic matrices of the center, left contact, and right contact atoms, thereby linking the interatomic potentials to the transmission function. A detailed description of the calculation procedure is available in [85].

AGF is increasingly being used to study the interaction of phonons with extended structures. For example, AGF has been able to shed light on phonon scattering by nanoparticles. While nanoparticles have long been known to reduce thermal conductivity by scattering phonons [107], the modeling of this scattering process has traditionally been based on an interpolation between Rayleigh and geometrical scattering limits within the framework of continuum acoustics [108]. However, for sufficiently small wavelengths the discreteness of the atomic lattice must be taken into account. Kundu *et al* used AGF with *ab initio* force fields to exactly calculate the scattering rate from nanoparticles to all orders, finding that nanoparticles composed of heavier atoms than those of the host lattice can provide a larger reduction in thermal conductivity than with lighter particles, as shown in figure 3(*b*). This result cannot be predicted from the Born approximation. However, the calculations also revealed that the scattering rates based on continuum acoustics were within 20% of the exact values, providing rigorous justification for the use of these simpler models.

Another key process for which AGF has been employed is computing phonon transmission and reflection at semiconductor-semiconductor interfaces. This process is particularly important as interfaces exist in many applications such as quantum well lasers [1]. Numerous previous works have studied phonon transport across clean and rough interfaces; for example, Zhao and Freund studied transport across rough interfaces of fcc lattices [109], Saltonstall *et al* examining the effect of adhesion and impurity mass on interfacial transmission [110], and Merabia and Termentzidis used molecular dynamics to compute the interface conductance between solids [111], among many other works [86, 94, 102–104, 112–115].

Recently, Tian *et al* used AGF to study phonon transmission across ideal and rough heterogeneous Si/Ge interfaces using both *ab initio* and empirical force fields [116]. The roughness was incorporated by mixing atoms near the Si/Ge interface. Traditionally, atomically smooth interfaces have been assumed to allow phonons to transmit with minimal reflection and hence possess the lowest thermal boundary resistance compared to rough interfaces. However, the AGF calculations revealed that certain types of rough interfaces could actually increase the transmission of mid-range phonon frequencies because atomic mixing softens the impedance mismatch between Si and Ge. Figure 3(*a*) shows the calculated transmittance from Si to Ge, demonstrating that interfaces with a small amount of interfacial mixing can increase the interfacial transmittance and hence reduce the thermal boundary resistance below the value for an atomically smooth interface. This nonintuitive result highlights the utility of AGF for studying phonon interactions with extended structures.

Combining AGF and *ab initio* calculations enables theoretical predictions to be directly compared to experiment without any fitting parameters and thus provides both experimental confirmation of the theory as well as deeper insight into the experiments. Such an approach was recently implemented by Chen *et al* in their computational and experimental study of SiGe superlattices [117]. These structures have long been of interest as they are a simple system that can be used to verify theoretical predictions regarding phonon interface scattering [77, 104, 112–115], and particularly whether superlattices can achieve the long-standing goal of thermal conductivities lower than the alloy limit. However, defects due to lattice mismatch between Si and Ge complicated the comparison of experimental measurements to theoretical predictions [118–121], leaving the thermal conductivity reduction achievable with superlattices subject to question.

Chen *et al* used molecular beam epitaxy to grow defect-free superlattices and measured the thermal conductivity using two methods. As shown in figure 3(*c*), the measured thermal conductivities of $2\,\mathrm{W\,mK^{-1}}$ were lower than those of the corresponding alloy and thus broke the alloy limit. Interestingly, and unexpectedly, the thermal conductivities of the actual samples, which exhibited non-abrupt intermixed interfaces as schematically shown in the inset of figure 3(*d*), were also lower than those expected for an abrupt superlattice in which the layers abruptly switch composition.

Prior to the introduction of the computational methods described in this section, unambiguously explaining these observations would be difficult. However, the authors were able to provide a microscopic account of the experimental results using the BTE with *ab initio* input and using AGF to obtain the point defect and interface scattering rates. From these calculations, the authors found that the actual superlattices have lower thermal conductivity than either the pure alloy or abrupt superlattice precisely because they contain both point defects and interfaces, thereby scattering a broader bandwidth of the phonon spectrum that is possible with only one of the scattering mechanisms. As shown in figure 3(*d*), diffused Ge atoms serve as point defects to efficiently scatter high frequency phonons while the barriers scatter low frequency phonons, and the presence of only one of these scattering mechanisms, as in the pure alloy or abrupt superlattice case, leaves a large portion of the phonon spectrum weakly scattered. The calculated results were in quantitative agreement with the experiments, as in figure 3(*c*). This study nicely demonstrates how the advances in computation described in this review have enabled new microscopic insights into a material that had previously been studied extensively both experimentally and computationally.

3.3. Variance-reduced Monte Carlo algorithms

Atomistic approaches have an advantage in that they require no adjustable parameters, but they are very computationally costly and cannot be applied to domains larger than a few nanometers. Simulating thermal transport in larger structures therefore requires a mesoscale treatment based on the BTE. Essentially all solutions of the BTE for problems involving temporal variations or non-uniform spatial gradients assume the RTA, with the governing equation given by equation (4). This form of the equation is considerably simpler than equation (2), and a number of approaches exist to solve equation (4). For example, exact analytical solutions can be obtained using integral transforms in infinite or semi-infinite

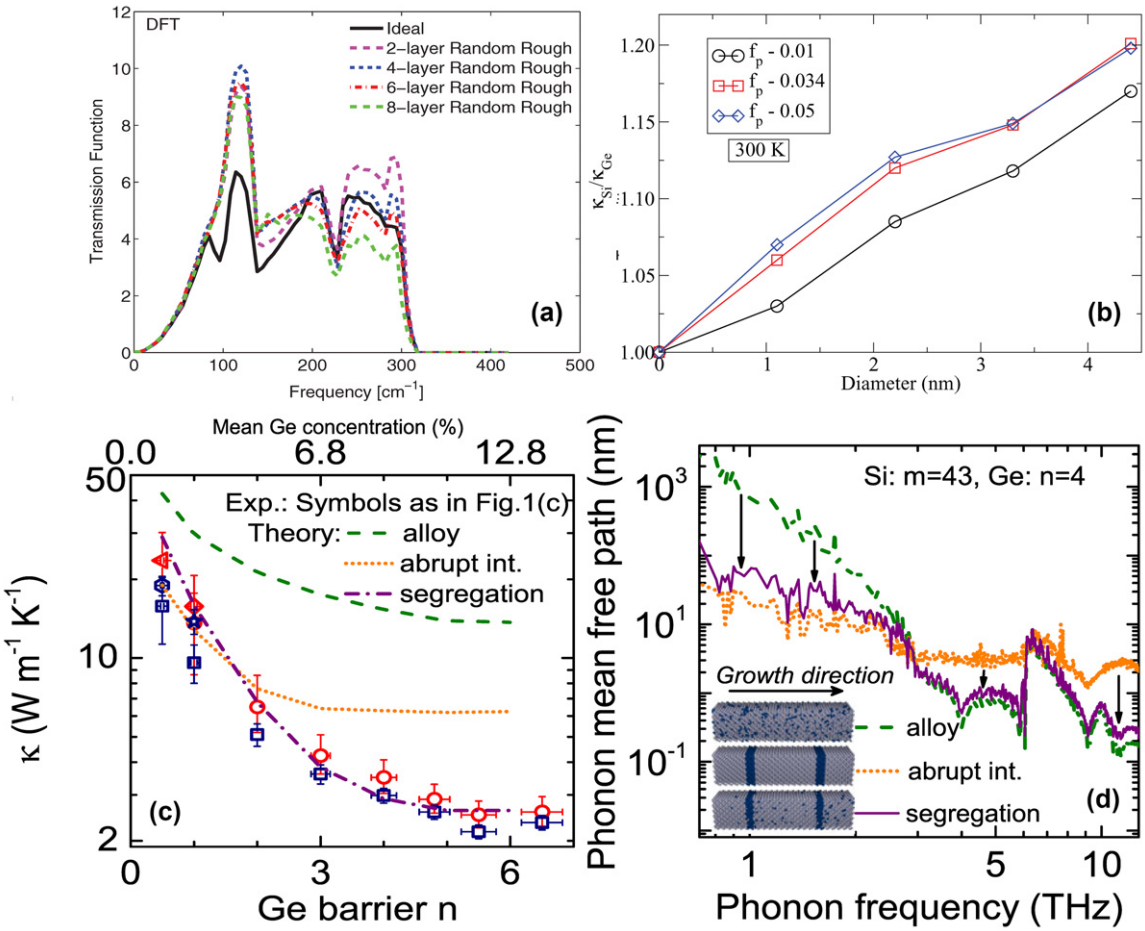

Figure 3. (*a*) Transmittance from Si to Ge calculated using AGF with DFT force constants. Interfaces with atomic mixing, denoted 'rough' interfaces, can enhance transmission across an interface. Reprinted figure 2 with permission from [116]. Copyright (2012) by the American Physical Society. (*b*) Ratio of thermal conductivity of a $Si_{0.5}Ge_{0.5}$ alloy with Si nanoparticles to that with Ge particles versus nanoparticle diameter. Several different nanoparticle concentrations f_p are shown. Lighter nanoparticles composed of Si yield a higher thermal conductivity than heavier Ge nanoparticles of the same size. Reprinted figure 2 with permission from [99]. Copyright (2011) by the American Physical Society. (*c*) Thermal conductivity versus number of Ge monolayers *n* (equivalent Ge concentration shown on top axis). The measured thermal conductivities (symbols) are much lower than those of either the pure alloy (green dashed line) or abrupt superlattice (orange dotted line) and quantitatively agree with *ab initio* calculations. (*d*) Phonon mean free paths versus frequency for the alloy (green dashed line), abrupt interface superlattice (orange dotted line), and the actual segregated superlattice (solid purple line). The phonon mean free paths in the segregated sample are uniformly low over the full range of phonon frequencies. (*c*) and (*d*) adapted from [117].

domains [122, 123]. We have recently reported a solution for an infinite domain including frequency dependence of phonon properties [124], and Collins *et al* reported solutions for different spectral models [125]. However, in many realistic situations a numerical solution is required. The most straightforward strategy is simply to apply finite differences to the derivatives, discretize the integrals, and solve the equation numerically, an approach known as discrete ordinates [32]. This approach for phonons was reported by Majumdar in a 1D geometry [108, 126]. Recently, discrete ordinates has been used to simulate steady 2D transport under the grey approximation [127] and 1D transient transport including frequency dependence of phonon properties [128]. However, discrete ordinates is challenging to apply to multiple spatial dimensions while including frequency dependence due to the substantial memory requirements. Other approaches taken in the thermal transport field include a two-flux method [129–131], Monte Carlo [132–138], finite volume [139–141], a mean free path sampling algorithm [142], and a lattice Boltzmann solver [143]. However, these algorithms are either computationally costly or make simplifying approximations that limit the validity of the solution.

Recently, variance-reduced Monte Carlo (MC) algorithms have been introduced that solve the BTE many orders of magnitude faster than other algorithms in complex 3D geometries while rigorously including frequency-dependence [144–147]. These deviational variance-reduced algorithms were originally introduced to simulate rarified gas dynamics [148, 149] and have been adapted for phonons by Radtke, Peraud and Hadjiconstantinou [144–146]. Further details of this method are described in a recent review [150]. These algorithms enable the BTE under the RTA to be rigorously solved without approximation in complex, large domains of size exceeding 1 mm and as a result enable the simulation of heat conduction in structures that were very challenging with prior numerical schemes.

To understand the principle underlying the deviational algorithm, consider a calculation of the spatial heat flux in an infinite domain with a fixed, localized temperature rise at 301 K while the rest of the domain is at 300 K. With traditional MC, this problem would be treated by discretizing the domain into cells and adding computational particles representing phonons into each cell with a Bose–Einstein distribution at the local temperature. Particles are present in every cell, and the desired heat flux is calculated by advecting and scattering the particles while sampling the heat flux in each cell after the system reaches steady state.

While this algorithm is the typical one used in many studies, it is clearly inefficient in many respects. First, the difference between a Bose–Einstein distribution at 301 K and 300 K is extremely small, meaning tremendous numbers of particles are required to adequately resolve the difference in the presence of stochastic noise due to number fluctuations of the particles. Second, in a sufficiently large computational domain that is not subject to artificial boundary effects most of the domain is at 300 K, meaning that most phonons present are not used to simulate the thermal transport process of interest but rather are needlessly reproducing a 300 K Bose–Einstein distribution that is known analytically. This unnecessary computation dramatically increases the memory requirements, computational effort, and stochastic noise of the simulation.

Deviational MC algorithms are based on this key observation: there is no need to stochastically simulate a quantity, like the Bose–Einstein distribution, that is known analytically. In deviational MC this deterministic information is incorporated into the simulation by letting computational particles represent deviations from the given equilibrium distribution, in this example a Bose–Einstein distribution at 300 K, rather than actual phonons as in traditional MC. Because both positive and negative deviations from the equilibrium distribution can occur, deviational particles also possess a sign. Besides this change, however, the simulation process proceeds largely as in traditional MC: particles are advected, scattered, and sampled to obtain the desired thermal quantity such as temperature and heat flux.

This small change in the algorithm drastically improves the computational efficiency in several critical ways. First, while in traditional MC particles are required in every cell, in deviational MC no particles are present if the cell is at the equilibrium temperature. Thus the only particles present in a deviational MC simulation are used to simulate the thermal transport process of interest. Further, deviational MC can resolve arbitrarily small temperature gradients because particles represent deviations from an equilibrium distribution rather than an absolute quantity. This ability is in marked contrast to traditional MC for which computational cost increases rapidly with decreasing temperature gradients.

Note that the deviational algorithm is always applicable regardless of the magnitude of the temperature gradient. However, it is most efficient compared to traditional MC when the maximum temperature variation over the domain ΔT is much smaller than the equilibrium temperature T [147], with the efficiency enhancement improving as $(T/\Delta T)^2$. For the example given above in which $\Delta T = 1\,\mathrm{K}$ and $T = 300\,\mathrm{K}$, the efficiency improvement is on the order of 10^5 compared to traditional MC algorithms, and thus a simulation that would take more than a day with traditional MC can be run in 1 s with deviational MC. An example of the low stochastic noise result that can be obtained is shown in figure 4(*a*), showing the two dimensional temperature profile of a slab with square pores calculated by Peraud *et al* [146]

In the case when $\Delta T/T \ll 1$, which often occurs in practice, an additional simplification can be made that further reduces the computational cost [144]. In this situation, the distribution to which scattering phonons relax, Ψ^0_λ, is nearly the same everywhere in the domain due to the small temperature differential, allowing Ψ^0_λ to be linearized. This linearization decouples the computational particles, allowing them to be simulated completely independently from each other and without any need for temporal and spatial discretization. This decoupling simplifies parallelization and reduces computational cost and memory requirements by orders of magnitude. Unlike the original deviational algorithm, though, this linearized algorithm is only applicable in the limit $\Delta T/T \ll 1$ due to the linearization of the Bose–Einstein distribution.

These algorithms, and the latter linearized algorithm in particular, are enabling new insights into mesoscale thermal transport that have not been previously possible due to computational limitations. For example, Peraud and Hadjiconstantinou demonstrated the efficiency of their algorithm by performing the first fully 3D simulations of a common optical experiment, time-domain thermoreflectance (TDTR), to microsecond time scales, as shown in figure 4(*b*) [144]. We have also implemented this simulation to better understand recent observations of quasiballistic transport using variable pump-size TDTR measurements [153].

In our group, we are using these algorithms to study a number of problems. For example, we have examined the origin of exceptionally low thermal conductivities in silicon nanomeshes consisting of periodic holes etched in a thin membrane [154, 155]. The measured thermal conductivities were apparently too low to be explained by boundary scattering and thus tentatively attributed to coherent phonon interference. Other works attempted to simulate phonon transport in these structures using the BTE but could only incorporate two dimensions [137] or modeled the scattering with a phenomenological scattering rate that lacked predictive power [156].

Using variance-reduced MC algorithms, we examined the origin of these observations by simulating the full 3D geometry of the nanomeshes while rigorously including the frequency-dependence of phonon properties [151]. As shown in inset of figure 4(*c*), we simulated thermal transport through one unit cell of a nanomesh with circular and square pores using periodic heat flux boundary conditions [137] and diffuse boundary scattering from pore walls and top and bottom boundaries. Our calculation demonstrated that the heat carried by low frequency modes that were most likely to undergo coherent interference was not sufficient to explain the observed low thermal conductivies of 1–2 $\mathrm{W\,mK^{-1}}$. As shown in figure 4(*c*), most of the heat in nanomeshes

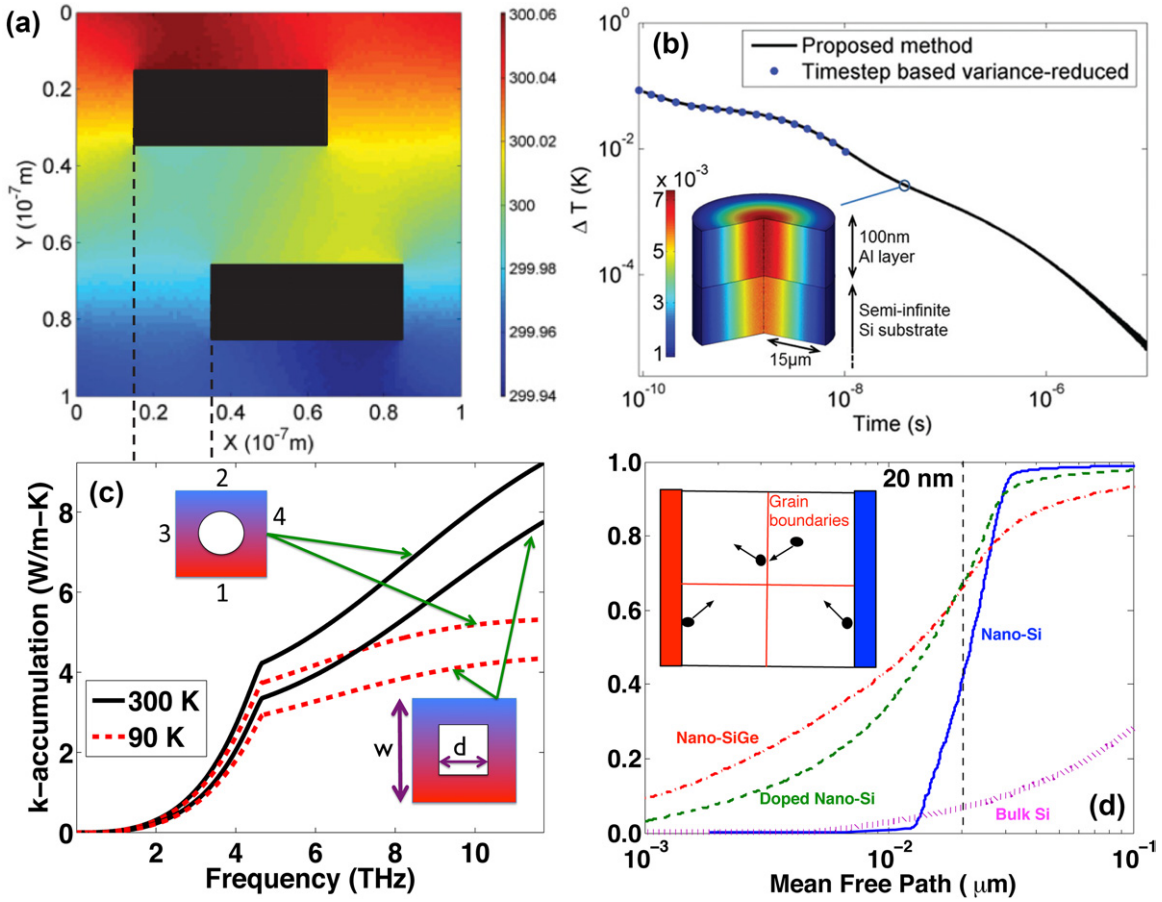

Figure 4. (*a*) Temperature field of silicon with displaced rectangular pores subject to a small temperature gradient, demonstrating extremely low stochastic noise. Reprinted figure 10 with permission from [146]. Copyright (2011) by the American Physical Society. (*b*) Calculation of surface temperature versus time in the geometry of a TDTR experiment, consisting of a film on a substrate with a Gaussian radial initial temperature distribution in the film. The more efficient linearized algorithm [144] can calculate the temperature decay to microsecond time scales with little stochastic noise, compared to nanosecond time scales possible with the original algorithm. Reprinted with permission from [144]. Copyright (2012), AIP Publishing LLC. (*c*) Spectral thermal conductivity accumulation versus phonon frequency for a nanomesh, or a thin silicon membrane with circular or square periodic pores. The heat carried by low frequency phonons that could undergo coherent interference is not sufficient to explain the exceptionally low thermal conductivities of 1–2 W mK^{-1} reported in nanomeshes [151]. (*d*) MFP accumulation function for nanocrystalline silicon with a 20 nm grain size including a frequency-dependent grain boundary scattering rate. Due to the frequency-dependent scattering, long MFP phonons still contribute substantially to heat conduction despite the presence of grain boundaries [152]. Inset: 2D illustration of the 3D simulation geometry, consisting of periodic heat flux boundary conditions (left and right sides) to simulate one repeating unit of the material, and grain boundaries (red lines) in a 3D cubic geometry. Computational particles (black circles) are reflected or transmitted at the grain boundaries.

is carried by phonons with frequencies larger than 3 THz, corresponding to wavelengths of less than two nanometers. These wavelengths are very small compared to the reported periodicity of 10–20 nanometers, thus making coherent effects unlikely to affect heat conduction. Instead, the low thermal conductivities could be accounted for by the presence of a 2–3 nm thick native oxide that effectively increased the pore size as well as phonon backscattering at the pore walls. Our calculations demonstrate that thermal phononic crystals designed for operation at room temperature must have periodicity on the order of 1–2 nanometers and atomic level roughness, a difficult fabrication requirement at present. However, as recently reported by Zen *et al* thermal phononic effects can occur at sub-K temperatures even with micron-sized structures because of the increase in thermal phonon wavelength at these low temperatures [157].

We have also used these algorithms to study thermal transport in nanocrystalline silicon with a realistic 3D grain structure [152]. A recent experimental work by Wang *et al* provided evidence that the scattering rate due to grain boundary scattering in nanocrystalline silicon is not grey, as typically assumed, but must depend on the phonon frequency [158]. We wanted to examine the impact of the frequency-dependent grain boundary scattering on the distribution of heat in the thermal phonon spectrum. While a phenomenological scattering rate $\tau^{-1} = v/L$ can be used along with an analytic solution of the BTE to obtain some insight, this approach lacks predictive power because in the non-grey model the geometrical length L depends on phonon frequency and is not known in advance. Instead, we modeled phonon transmission across the grain boundary and exactly incorporated the geometrical effects using the linearized MC algorithm with a cubic, 3D grain structure and periodic heat flux boundary conditions [137]. Phonon scattering at the grain boundary was simulated by generating a random number and comparing it to the transmissivity for the relevant phonon frequency. If

the random number was smaller than the transmissivity the phonon was transmitted; otherwise it was reflected.

We found that the transmissivity required to explain the measurements of Wang *et al* increased with decreasing phonon frequency, approaching unity as the phonon frequency tended to zero. As a result, our model predicted that a large fraction of heat is carried by low frequency phonons with MFPs exceeding the grain size. Figure 4(*d*) shows the accumulated thermal conductivity versus phonon MFP, demonstrating the large contribution from long MFP phonons despite the presence of the grain boundary. Our results suggest that long MFP phonons may still contribute substantially to heat conduction in nanocrystalline materials, with important implications for improving the efficiency of thermoelectrics.

Many other interesting studies lie ahead using these powerful algorithms. When combined with the previously described first-principles and atomistic level modeling techniques, these algorithms enable predictive simulations of thermal transport in realistic, multidimensional structures without any adjustable parameters.

4. Experiment

Experimentally measuring the transport properties of specific phonons has been a considerable challenge. This capability is all the more important considering that computational methods are now providing detailed, specific predictions regarding quantities such as the MFP spectrum, as described in the previous section, that must be verified with experiment. However, direct experimental measurements on the thermal phonon spectrum are essential in their own right as they too provide results that can drive computations. Further, some complex materials with a large number of atoms in the unit cell, for example $Yb_{14}MnSb_{11}$ [159], remain computationally intractable, leaving experiment as the only option to obtain a microscopic view of heat conduction. Here, we describe the new views of phonon transport provided by two experimental techniques, inelastic neutron scattering (INS) and a new method called mean free path spectroscopy.

4.1. Inelastic neutron scattering

INS has been used for decades in condensed matter physics to measure phonon dispersions by observing the interaction of a neutron with a phonon [160–163]. Recently, INS has emerged as a powerful technique to provide microscopic measurements of the transport properties of phonons [12, 164, 165]. By leveraging a number of technical advances, INS can now be used to map phonon modes and relaxation times over the entire Brillouin zone in single crystal samples.

In early INS implementations, continuous neutron fluxes and triple-axis spectrometers were used to serially map the scattering function versus wavevector and energy. This approach requires substantial beam time, restricting studies to high symmetry lines in the crystal. Recent advances in pulsed spallation sources, time-of-flight neutron spectrometers, and large-area detectors now allow a wide range of wavevectors to be measured simultaneously, dramatically reducing the beam time needed for measurements. Further, advances in software allow the full 4D scattering function $S(\mathbf{q}, E)$ to be reconstructed from several measurements with different crystal orientations. Finally, a better ability to correct for instrumental broadening and multiple scattering effects enables the phonon linewidths Γ, and therefore relaxation times $\tau = 1/2\Gamma$ or scattering rates τ^{-1}, to be accurately measured.

These advances were first applied to PbTe, historically an excellent thermoelectric material with very low lattice thermal conductivity [164]. However, the microscopic origin of this low thermal conductivity remained unclear. Using INS, Delaire *et al* mapped the full Brillouin zone of PbTe and uncovered an interesting feature of the phonon dispersion. While harmonic DFT calculations predict the LA and TO modes to cross, INS measurements revealed the presence of an extended avoided crossing as schematically shown in figure 5(*a*), indicating a strong anharmonic repulsion between the branches. This strong scattering was also reflected in the phonon linewidths, which exhibited a peak in the LA branch at certain frequencies due to the interaction as in figure 5(*b*). The INS measurements thus demonstrated that the low thermal conductivity of PbTe can be attributed in large part to the extremely strong damping of the LA branch by the LA–TO interaction. It is interesting to note that previous DFT calculations and INS measurements were unable to identify this avoided crossing, demonstrating the unique results provided by advances in the INS technique.

Subsequently, INS was used by Ma *et al* to study $AgSbTe_2$ [12, 166]. The unusual thermal conductivity of this material was originally reported by Morelli *et al* [167] and is puzzling because it is clearly a crystal, as evidenced by x-ray diffraction, yet its thermal conductivity follows the trend of a glass rather than that a crystal, with a slow increase of thermal conductivity with temperature. Morelli *et al* originally attributed this observation to extreme anharmonicity that arises from the bonding configuration of the compound.

Ma *et al* applied a number of experimental techniques to this material, including INS, to provide a detailed microscopic account of the thermal conductivity of $AgSbTe_2$. As was performed for PbTe, the authors mapped the scattering function and linewidths over the full Brillouin zone and again found interesting features. In $AgSbTe_2$, the linewidths are extremely broad, even in comparison to PbTe, with the upper part of the LA and optical branches so broad that they merge into a continuum. However, no temperature dependence of linewidths was observed, demonstrating that anharmonicity could not be responsible for the low thermal conductivity as it was for PbTe. Because the scattering rate due to point defects was also calculated to be too weak, the INS measurements showed that another defect structure must be responsible.

The authors used transmission electron microscopy (TEM) to confirm the presence of this defect structure in the form of ordered nanodomains that spontaneously form over length scales of a few nanometers, values that are consistent with the phonon MFPs determined from the measured linewidths as shown in figure 5(*c*). DFT calculations showed that the reason for this spontaneous nanostructure is a degeneracy in ground state crystal structure energy. It is

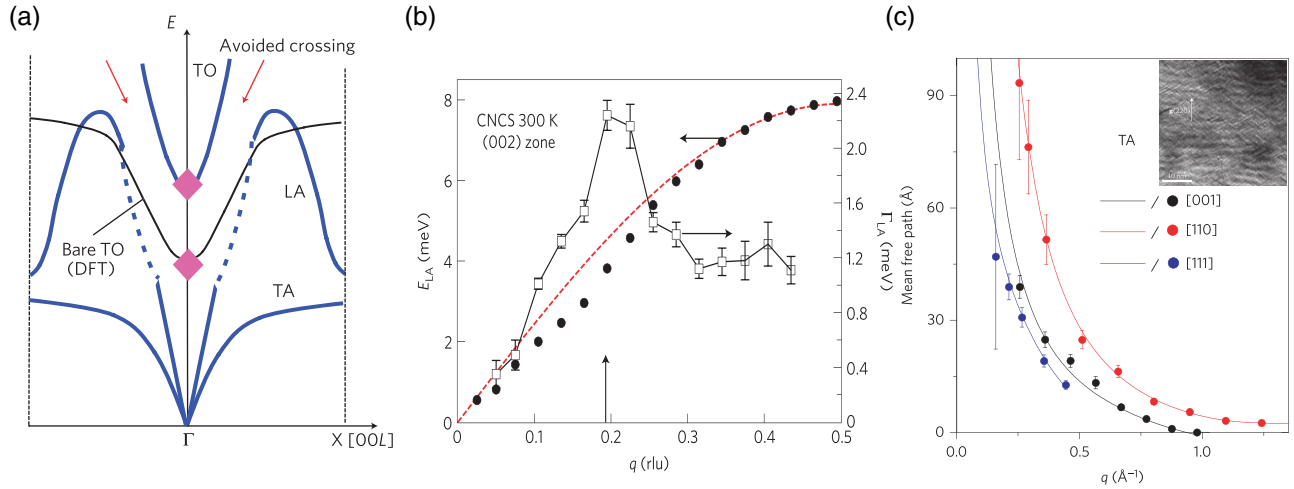

Figure 5. (*a*) Schematic illustration of the avoided crossing that occurs in PbTe due to strong anharmonic interactions between the LA and TO modes. The solid blue lines represent the actual dispersion, the pink diamonds indicate measurements obtained with INS, and the solid black lines represent harmonic DFT calculations that describe the phonon dispersion in the absence of anharmonicity and thus do not predict the avoided crossing. Reprinted by permission from Macmillan Publishers Ltd: Nature Materials, [164], Copyright (2011). (*b*) Measured dispersion and linewidths of the LA mode in PbTe [164], demonstrating a peak in the linewidth corresponding to a large scattering rate. Reprinted by permission from Macmillan Publishers Ltd: Nature Materials, [164], Copyright (2011). (*c*) Measured transverse acoustic branch (TA) phonon MFPs versus wavevector of $AgSbTe_2$ along different crystallographic directions. The MFPs are remarkably short and of the order of the size of the nanodomains, shown in the TEM image in the inset. Reprinted by permission from Macmillan Publishers Ltd: Nature Nanotechnology, [12], Copyright (2013).

these nanodomains that are responsible for the low thermal conductivity, scattering phonons so strongly that the thermal conductivity approaches the amorphous limit. The authors noted that this spontaneous nanostructure may be useful for thermoelectrics because it is thermodynamically stable, unlike artificial nanostructures that are often metastable.

These two studies illustrate the utility of INS to provide an experimental microscopic view of thermal transport. Not only are the results of fundamental scientific interest, they also guide the development of more efficient thermoelectric materials.

4.2. Mean free path spectroscopy

INS, while a powerful technique, does have limitations. It is best suited for single crystals samples for which the full Brillouin zone can be mapped. Additionally, low energy phonons, which have recently been demonstrated to play an essential role in heat conduction [56, 82], are difficult to study with INS due interference from the elastic scattering peak.

Fortunately, a considerably simpler experimental technique has emerged in the past several years that enables the first direct MFP measurements over a wide range of length scales and materials using readily available equipment. The technique, mean free path spectroscopy [168], is able to directly measure the MFP accumulation function, defined as the accumulated thermal conductivity as a function of phonon MFP [169, 170]. This distribution contains less information than INS measurements on single crystals but still provides extremely useful insights into which phonons are the primary heat carriers and the key length scales at which a material's thermal conductivity decreases from its bulk value due to scattering from grain boundaries or sample boundaries. Further, the technique can be applied to most solids, including complex materials such as polycrystals or nanocomposites.

Mean free path spectroscopy is based on a simple principle: the heat flux dissipated by a given temperature difference depends on how a thermal length scale, or the distance over which a temperature difference exists, compares with the MFPs [171]. If the thermal length is much larger than the MFPs, the heat transport is diffusive and accurately described by Fourier's law. At the other extreme, when the thermal length is much smaller than the MFPs, phonons move ballistically, and heat transport occurs by phonon radiation in an exact analogy to thermal radiation from a blackbody [132]. As the thermal length decreases and more of the phonon spectrum transports heat ballistically, Fourier's law gradually breaks down. As schematically illustrated in figure 6, MFP spectroscopy consists of observing the discrepancies in heat flux from the Fourier's law prediction as the thermal length is systematically varied from the diffusive to ballistic regimes.

It is instructive to compare the principle of MFP spectroscopy with previous efforts to infer MFPs by changing the physical dimensions of a sample. For example, Ju and Goodson reported thermal conductivity measurements of Si membranes with variable thickness, from which information about MFPs was obtained by correlating the dimensions of the sample with the thermal conductivity value [172]. The key insight of MFP spectroscopy is that one need not change the dimensions of the sample to probe MFPs. Instead, varying the length scale over which heat is transported in a macroscopic material allows the same information to be obtained and without the additional complication of boundary scattering. This insight is essential because it allows the thermal length to be externally controlled and applied to a wide variety of samples with essentially no change in experimental setup.

MFP spectroscopy can be implemented with different experimental methods so long as a thermal length can be

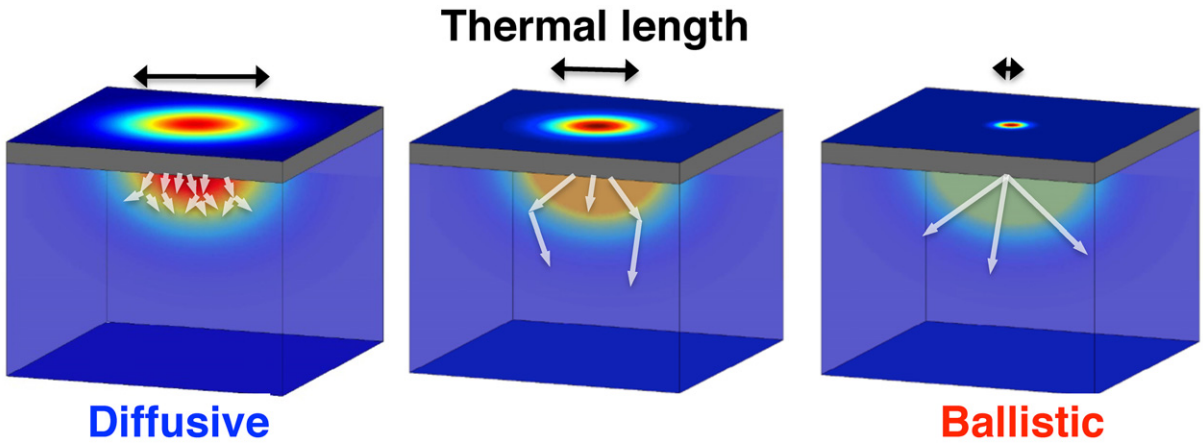

Figure 6. Schematic of the physical principle underlying the MFP spectroscopy technique. The heat flux dissipated by a fixed temperature difference is very different depending on the thermal length relative to phonon MFPs, denoted by the lengths of the white arrows. MFP spectroscopy consists of systematically observing the transition from the diffusive to the ballistic regimes by varying a thermal length scale, from which the underlying MFP distribution can be obtained.

externally defined and systematically varied over length scales comparable to MFPs. For example, previous works have used a variable heating laser beam diameter [168] or, as discussed in more detail below, the fringe spacing of two interfering laser beams [173]. The discrepancies in heat flux are observed as an effective thermal conductivity that deviates from the bulk value and appears to vary with the thermal length. Note that this effective thermal conductivity is not an intrinsic property of the bulk material but depends both on material properties, particularly the phonon MFP spectrum, and the spatial heating profile.

The introduction of MFP spectroscopy is quite recent, although the possibility of using observations of nondiffusive transport to infer phonon relaxation times was raised as early as 1971 [174]. More recently, Koh and Cahill observed a modulation-frequency dependent thermal conductivity in semiconductor alloys using TDTR and attributed it to ballistic transport [175]. Subsequently, Siemens *et al* reported the observation of strongly nondiffusive transport in nickel nanolines patterned on a sapphire substrate, which was attributed to a ballistic thermal boundary resistance [176]. Shortly thereafter, Minnich *et al* described the principle of MFP spectroscopy based on observations of a pump-size dependent thermal conductivity in silicon at cryogenic temperatures using TDTR [168]. Johnson *et al* used transient grating spectroscopy to determine MFPs in Si membranes [173]. Regner *et al* reported an approach for MFP spectroscopy using a new experimental setup called broadband-frequency domain thermoreflectance (BB-FDTR) [177, 178].

To quantitatively understand the physics of MFP spectroscopy, consider a transient grating spectroscopy experiment (TG) in which a sample is impulsively heated with a sinusoidal pattern of variable spatial period created by the interference of two laser beams [179, 180]. The transient thermal decay is measured using a probe laser, and the in-plane thermal conductivity is extracted as the only unknown parameter in a thermal model used to fit the decay curve. This experiment is implemented in our lab using a microchip laser as pump (532 nm, 1 ns duration, 1 kHz repetition rate) and a CW laser (Coherent Genesis, 0.5 W, 514 nm) as probe. The probe is chopped to reduce steady heating. The pump is focused onto a phase mask, or a custom diffractive optic, to split it into ± 1 diffraction orders. These two beams are collimated and focused onto a sample by two achromats, where the laser pulses interfere to form a sinusoidal intensity pattern with a spatial period defined by the crossing angle. The sample absorbs this light and is heated according to the spatial pattern, creating a sinusoidal variation in the dielectric constant and surface displacement. For detection, the probe follows exactly the same path as the pump, and on reaching the sample the probe diffracts from the periodic grating on the sample created by the pump excitation. The diffracted light is detected in real time using a fast photodiode and an oscilloscope with 500 MHz bandwidth, yielding the transient temperature decay of the surface, from which the thermal diffusivity is obtained by extracting the exponential time constant of the thermal decay.

Johnson *et al* used a similar version of this experiment in the lab of Prof. Keith Nelson at MIT to study thin silicon membranes with thicknesses of a few hundred nanometers [173]. Some of the experimental data are shown in figure 7(*a*) and consist of simple exponential decays with time constants that depend on the grating period and the thermal conductivity. The thermal conductivity measurements, normalized to the bulk value of silicon, extracted from these decay curves are shown in figure 7(*b*), and exhibit an unexpected trend. While the intrinsic thermal conductivity of a solid is a material property and therefore should be a constant, the data show a substantial decrease when the spatial grating period is smaller than 5 microns.

This observation can be explained by accounting for the possibility that some phonons have MFPs exceeding the grating period, resulting in nondiffusive thermal transport. Recently, we used the BTE to simulate the thermal transport that occurs in this experiment [124, 181]. The key observation from this work is shown in figure 7(*c*), which plots the calculated spectral heat flux versus the MFP in the TG geometry. While Fourier's law predicts that long MFP ballistic phonons contribute substantially to heat conduction,

the calculated heat flux from phonons with MFPs comparable to the spatial grating period is smaller than this prediction. It is this discrepancy in the heat flux between what Fourier's law predicts and what actually occurs in the experiment that is the origin of the effective thermal conductivities that appear to depend on thermal length scale [173]. Quantitatively, the discrepancy can be described by a suppression function, also shown in the figure, that depends primarily on the experimental geometry.

Confusion often arises with the statement that the ballistic heat flux is less than the Fourier's law prediction. Intuitively, one expects that in the ballistic regime the heat flux should be larger than in the diffusive case due to the absence of scattering events. Here, one must be very careful about precisely what is being compared. Consider two thermal reservoirs at different, fixed temperatures connected by a crystal with some thickness. When the crystal is made thinner and scattering events become less likely, the heat flux does increase, eventually reaching the ballistic limit in which heat is transported by phonons at the group velocity without scattering. This ballistic limit is the maximum heat flux that can be supported in the material. However, applying Fourier's law based on the thermal conductivity corresponding to the bulk material will predict a heat flux that exceeds this ballistic limit, even tending to infinity as the crystal thickness approaches zero. Clearly, it is not possible for a finite temperature difference to dissipate a nearly infinite heat flux, and under these conditions the actual ballistic heat flux is smaller than the Fourier law prediction, as stated above. While this example is strictly only valid for steady heat conduction between blackbodies, recent solutions of the BTE by us and others demonstrate that the same physical principle applies in every case, including transient transport, examined thus far [124, 125, 128, 153, 181, 182].

Mathematically, the observations from figure 7(*c*) can be expressed as:

$$\kappa_i = \int_0^\infty q_i K(q_i \Lambda_\omega) F(\Lambda_\omega) \mathrm{d}\Lambda_\omega \tag{11}$$

where κ_i are the measured effective thermal conductivities, $q_i = 2\pi/L_i$ is the TG wavevector and L_i is the grating period, $K(q_i \Lambda_\omega)$ is the derivative of the suppression function, Λ_ω is the MFP, and $F(\Lambda_\omega)$ is the desired MFP spectrum. Using this equation, we can explain the origin of the effective thermal conductivities that depend on thermal length scale, observations that have been reported previously by Maznev *et al* [182] and Hua and Minnich [124].

The key insight of MFP spectroscopy is that this equation can be used not just to explain experimental data but rather to directly measure the MFP spectrum. Instead of performing the calculation in the forward direction, or using a MFP spectrum to predict effective thermal conductivities, the equation can instead be flipped around to reconstruct the MFP spectrum from measurements of the effective thermal conductivities [181]. This reconstruction procedure is the essence of the MFP spectroscopy technique.

Unfortunately, implementing the procedure is not so straightfoward because equation (11) is a classic ill-posed inverse problem that does not possess a unique solution. Specifically, this equation is an inhomogeneous Fredholm integral equation of the first kind that appears often in deconvolution and similar inverse problems. This degeneracy complicates the recovery of the desired MFP distribution.

We were able to overcome this challenge by reformulating the problem as an optimization [181]. First, we discretize the integral using Gaussian quadrature to obtain a linear system of equations for the unknown MFP distribution F_j:

$$\kappa_i = \sum_{j=1}^{N} A_{i,j} F_j \tag{12}$$

where N is the number of integration points, $F_j = F(\Lambda_j)$ is the desired MFP distribution, $A_{i,j} = K(q_i \Lambda_j) q_i \beta_j$ has dimension $M \times N$ where M is the number of measurements, and Λ_j and β_j are the quadrature points and weights, respectively,

Second, we recall the basic constraints on F because it is a cumulative distribution function. Specifically, F is subject to the following restrictions: (1) $F(0) = 0$; (2) $F(\infty) = 1$; and (3) F is nonnegative and monotonically increasing. Also, the MFP distribution is unlikely to have abrupt steps because it is spread over such a wide range of MFPs and therefore F must obey some type of smoothness restriction.

Finally, we solve the problem by minimizing a penalty function P:

$$P = ||AF - \kappa||_2^2 + \eta ||\Delta^2 F||_2^2 \tag{13}$$

subject to the constraints described above. Here $\Delta^2 F = F_{j+1} - 2F_j + F_{j-1}$ is the second difference operator and $||\cdot||_2$ is the 2-norm. The first term on the right-hand side of equation (13) enforces that the solution satisfies equation (12), while the second term enforces smoothness in the solution. η controls the relative weight of the smoothness penalty. The solution is not sensitive to the particular value of η within a certain range. If η is too small, the solution will have unphysical jumps, while if η is too large the solution will not satisfy the linear system. Thus even though the solution does not possess a unique solution mathematically, in practice the actual MFP distribution can be found by incorporating simple physical constraints into the mathematical reconstruction procedure.

This calculation can be easily implemented using the freely available `CVX` package [183, 184]. An example result is shown in figure 7(*d*) in which we simulated the temperature decay of a transient grating using the BTE to obtain the effective thermal conductivities, then performed the reconstruction procedure to obtain the MFP distribution using our knowledge of the suppression function. We observed excellent agreement with the MFP distribution used in the BTE simulations, confirming the validity of this approach. This reconstruction approach has also been implemented experimentally [81].

The attractive feature of this reconstruction framework is that the BTE need not be solved every time one wants to explain experimental data. Instead, the BTE only needs to be solved once for a particular experimental geometry to extract the suppression function. Then, MFP spectra can be reconstructed using this function and the experimental measurements.

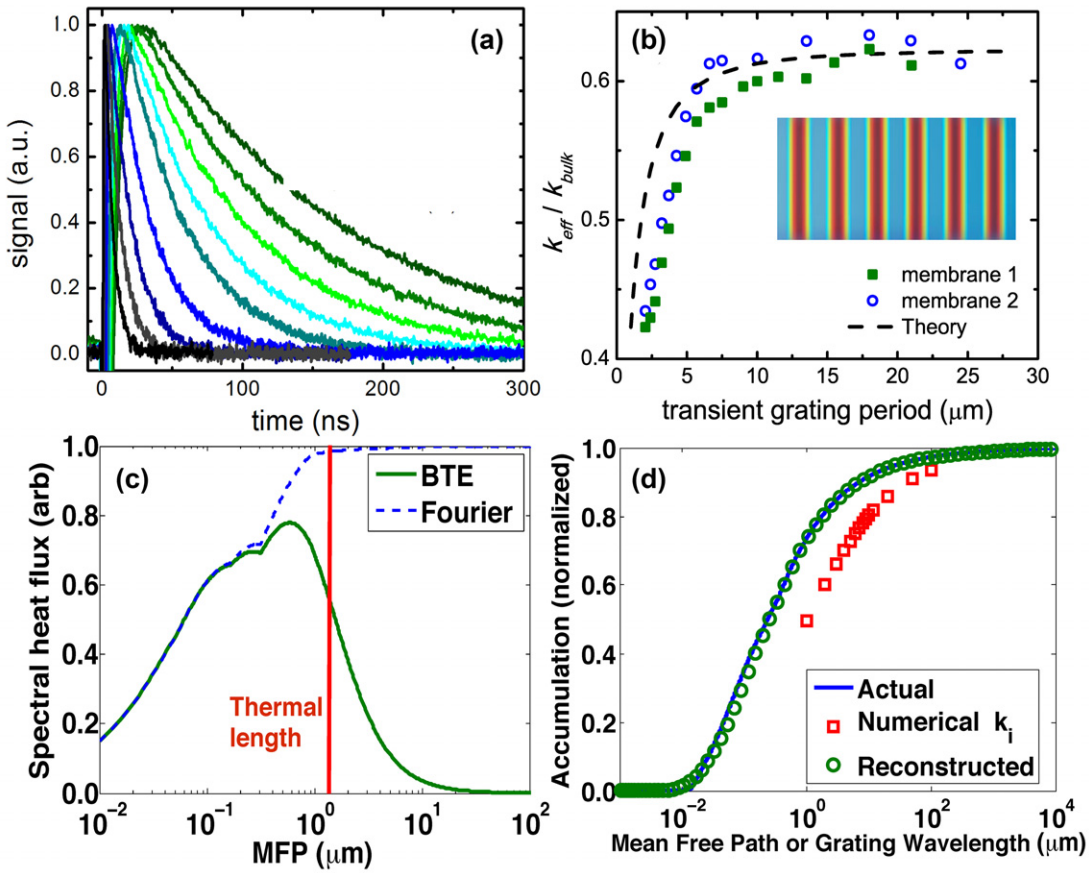

Figure 7. (*a*) Experimental measurements of the thermal decay of a 390 nm thick silicon membrane for several grating periods from 18 microns (slowest decay) to 3.2 microns (fastest decay) [173]. (*b*) Normalized thermal conductivity measurements, relative to the bulk silicon value, extracted from the thermal decays in (*a*). Symbols denote measurements on two separate membranes of similar thickness, while the dashed line denotes the theoretical prediction based on Maznev *et al* [182]. The effective thermal conductivity decreases rapidly when the grating period is smaller than 5 microns, indicating nondiffusive transport is taking place. Inset: illustration of the spatial heating profile created in TG. (*c*) Spectral heat flux versus MFP for the transient grating experiment obtained from an analytic solution to the BTE [124], demonstrating that phonons with MFPs comparable to the grating period (thermal length, red vertical line) have a reduced heat flux (green solid line) compared to the Fourier law prediction (dashed blue line). (*d*) Numerical example of the reconstruction procedure to obtain the MFP distribution. The effective thermal conductivities (red squares) are obtained from numerically synthesized data. Using these data and the procedure described in the text we reconstruct the MFP distribution (green circles), demonstrating excellent agreement with the actual MFP distribution (blue solid line).

While MFP spectroscopy is still a young technique, it has already provided a number of important insights into heat conduction. A particularly interesting result has been the confirmation of the importance of long MFP phonons to thermal transport in semiconductors despite their small contribution to specific heat, in agreement with predictions from first-principle calculations [56]. In bulk crystalline Si, MFP spectroscopy has shown that MFPs are hundreds of microns long even at 100 K [168]. The measurements of Johnson *et al* in figure 7(*b*) indicate that most thermal phonons scatter diffusely from membrane boundaries [173], an important insight for understanding boundary scattering in nanostructures. As the theory underlying MFP spectroscopy is refined, further novel results are expected to follow.

5. Summary and outlook

A fundamental microscopic understanding of phonon heat conduction has long been desired for both science and engineering but historically difficult to obtain due to limitations on computational and experimental methods. In this topical review, we have described how advances in a diverse set of techniques, most of which were introduced in the past five years, are enabling an unprecedented microscopic picture of thermal phonon transport from the atomistic level up to macroscopic dimensions. Examples of the insights obtained include the verification of theoretical predictions that low frequency phonons contribute substantially to thermal conductivity despite their small heat capacity, an understanding of the microscopic mechanisms underlying exceptionally good thermal conductors, and an improved understanding of phonon transmission across rough interfaces.

What is next for this microscopic investigation? Despite these advances, many aspects of heat conduction in the majority of materials remains unclear. Here, we describe a few of these important questions.

Our understanding of anharmonic scattering has been dramatically improved by *ab initio* calculations, but many predictions for materials ranging from nitrides to graphene remain to be experimentally verified. An important task

will thus be to use INS or MFP spectroscopy to directly measure microscopic quantities such as MFP spectra and compare the results to *ab initio* calculations. The agreement, or lack of agreement, will lead to a deeper understanding than that obtained from either method separately. An additional interesting topic for anharmonic scattering is understanding phonon interactions in materials with complex unit cells such as $Yb_{14}MnSb_{11}$ [159], for which numerous optical branches exist that could scatter acoustic phonons. The unit cells in such materials are so large that they may not be tractable with DFT at present, making an experimental approach the most promising option to gain insight into these materials.

After understanding anharmonic scattering, the next step is to investigate basic scattering mechanisms such as point defect scattering and electron–phonon scattering as they play an important role in thermoelectric materials. The scattering rate due to point defects can be derived from perturbation theory [38] but it has not been experimentally verified. Our understanding of electron–phonon scattering is more elementary, with most treatments being based in Ziman's original treatment from over 50 years ago that suggests that low energy phonons are scattered by electrons [35]. Again, this prediction has never been verified. INS or MFP spectroscopy could be used, although MFP spectroscopy can be more easily applied to a variety of materials.

Subsequently, the important task is to understand scattering due to extended defects such as grain boundaries, superlattice interfaces, nanoparticles, and other natural or artificial nanostructures. Despite the numerous demonstrations of nanostructured materials with reduced thermal conductivities, precisely which phonons are scattered by different defects remains unknown. Many other important questions remain; for example, what is the specularity parameter of phonons incident on a rough boundary? What is the phonon transmissivity at metal-semiconductor and semiconductor-semiconductor interfaces? What is the best way to incorporate all of these structures into a material to obtain the minimum thermal conductivity? Conversely, how can heat be most effectively extracted from a volume that includes interfaces, such as the active region of an LED?

The answers to these questions will have an important impact on the science and engineering of thermal conductivity. From a scientific perspective, knowledge of these microscopic details provides a predictive, fundamental understanding of the origin of thermal conductivity in solids that has been historically lacking. From an engineering perspective, this microscopic information provides the insights necessary to manipulate the thermal phonon spectrum for numerous applications ranging from thermoelectrics to LED lighting. The thermal transport field thus has an exciting time ahead as new tools are used to answer these fascinating and important questions.

Acknowledgments

The author thanks S Lee, L Zheng, Z Tian, J Garg and O Delaire for commenting on the manuscript. This work was sponsored in part by R Bosch LLC through Bosch Energy Research Network Grant no. 13.01.CC11, by the National Science Foundation under grant no. CAREER CBET 1254213, and by Boeing under the Boeing-Caltech Strategic Research & Development Relationship Agreement.

References

[1] Cahill D G *et al* 2014 Nanoscale thermal transport. II 2003–2012 *Appl. Phys. Rev.* **1** 011305
[2] Cahill D G, Ford W K, Goodson K E, Mahan G D, Majumdar A, Maris H J, Merlin R and Phillpot S R 2003 Nanoscale thermal transport *J. Appl. Phys.* **93** 793–818
[3] Pop E and Goodson K E 2006 Thermal phenomena in nanoscale transistors *J. Electron. Packag.* **128** 102–8
[4] Pop E 2010 Energy dissipation and transport in nanoscale devices *Nano Res.* **3** 147–69
[5] Yan Z, Liu G, Khan J M and Balandin A A 2012 Graphene quilts for thermal management of high-power GaN transistors *Nat. Commun.* **3** 827
[6] Su Z, Huang L, Liu F, Freedman J P, Porter L M, Davis R F and Malen J A 2012 Layer-by-layer thermal conductivities of the Group III nitride films in blue/green light emitting diodes *Appl. Phys. Lett.* **100** 201106
[7] Cho J, Li Z, Asheghi M and Goodson K E 2014 Near-junction thermal management: thermal conduction in gallium nitride composite substrates *Annual Review of Heat Transfer* (New York: Hemisphere)
[8] Biswas K, He J, Blum I D, Wu C-I, Hogan T P, Seidman D N, Dravid V P and Kanatzidis M G 2012 High-performance bulk thermoelectrics with all-scale hierarchical architectures *Nature* **489** 414–8
[9] Mehta R J, Zhang Y, Karthik C, Singh B, Siegel R W, Borca-Tasciuc T and Ramanath G 2012 A new class of doped nanobulk high-figure-of-merit thermoelectrics by scalable bottom-up assembly *Nat. Mater.* **11** 233–40
[10] Voneshen D J *et al* 2013 Suppression of thermal conductivity by rattling modes in thermoelectric sodium cobaltate *Nat. Mater.* **12** 1028–32
[11] Chowdhury I, Prasher R, Lofgreen K, Chrysler G, Narasimhan S, Mahajan R, Koester D, Alley R and Venkatasubramanian R 2009 On-chip cooling by superlattice-based thin-film thermoelectrics *Nat. Nanotechnol.* **4** 235–8
[12] Ma J *et al* 2013 Glass-like phonon scattering from a spontaneous nanostructure in AgSbTe2 *Nat. Nanotechnol.* **8** 445–51
[13] Poudel B *et al* 2008 High-thermoelectric performance of nanostructured bismuth antimony telluride bulk alloys *Science* **320** 634–8
[14] Debye P J W, Nernst W, Smoluchowski M, Sommerfeld A and Lorentz H A 1914 *Vorträge über die kinetische Theorie der Materie und der Elektrizität* ed B G Teubner (Leipzig: Teubner)
[15] Peierls R 1929 On the kinetic theory of thermal conduction in crystals *Ann. Phys.* **3** 1055
[16] Herring C 1954 Role of low-energy phonons in thermal conduction *Phys. Rev.* **95** 954–65
[17] Pomeranchuk I I 1941 On the thermal conductivity of dielectrics at temperatures higher than the Debye temperature *J. Phys.* **4** 259
[18] Klemens P G 1958 Thermal conductivity *Solid State Physics* ed F Seitz and D Turnbull (London: Academic)
[19] Holland M G 1963 Analysis of lattice thermal conductivity *Phys. Rev.* **132** 2461–71
[20] Callaway J 1959 Model for lattice thermal conductivity at low temperatures *Phys. Rev.* **113** 1046–51

[21] Steigmeier E F and Abeles B 1964 Scattering of phonons by electrons in germanium-silicon alloys *Phys. Rev.* **136** A1149–55

[22] Zebarjadi M, Yang J, Lukas K, Kozinsky B, Yu B, Dresselhaus M S, Opeil C, Ren Z and Chen G 2012 Role of phonon dispersion in studying phonon mean free paths in skutterudites *J. Appl. Phys.* **112** 044305

[23] Jeong C, Datta S and Lundstrom M 2011 Full dispersion versus Debye model evaluation of lattice thermal conductivity with a Landauer approach *J. Appl. Phys.* **109** 073718

[24] Zebarjadi M, Esfarjani K, Dresselhaus M S, Ren Z F and Chen G 2011 Perspectives on thermoelectrics: from fundamentals to device applications *Energy Environ. Sci.* **5** 5147–62

[25] Minnich A J, Dresselhaus M S, Ren Z F and Chen G 2009 Bulk nanostructured thermoelectric materials: Current research and future prospects *Energy Environ. Sci.* **2** 466–79

[26] Ravichandran J *et al* 2013 Crossover from incoherent to coherent phonon scattering in epitaxial oxide superlattices *Nat. Mater.* **13** 168–72

[27] Luckyanova M N *et al* 2012 Coherent phonon heat conduction in superlattices *Science* **338** 936–9

[28] Chen G 2005 *Nanoscale Energy Transport and Conversion* (New York: Oxford University Press)

[29] Tian Z, Lee S and Chen G 2013 Heat transfer in thermoelectric materials and devices *J. Heat Transfer* **135** 061605

[30] Luo T and Chen G 2013 Nanoscale heat transfer: from computation to experiment *Phys. Chem. Chem. Phys.* **15** 3389

[31] Feng T and Ruan X 2014 Prediction of spectral phonon mean free path and thermal conductivity with applications to thermoelectrics and thermal management: a review *J. Nanomater.* **2014** 1–25

[32] Chandrasekhar S 1950 *Radiative Transfer* (New York: Dover)

[33] Davison B and Sykes J B 1958 *Neutron Transport Theory.* 2nd edn (Oxford: Clarendon)

[34] Englman R 1958 The transport theory of temperature waves in insulators *Proc. Phys. Soc.* **72** 391

[35] Ziman J M 2001 *Electrons and Phonons: the Theory of Transport Phenomena in Solids* (Oxford: Oxford University Press)

[36] Srivastava G P 1990 *The physics of Phonons* (Boca Raton, FL: CRC Press)

[37] Broido D A, Malorny M, Birner G, Mingo N and Stewart D A 2007 Intrinsic lattice thermal conductivity of semiconductors from first principles *Appl. Phys. Lett.* **91** 231922

[38] Tamura S 1983 Isotope scattering of dispersive phonons in Ge *Phys. Rev.* B **27** 858–66

[39] Ward A, Broido D A, Stewart D A and Deinzer G 2009 *Ab initio* theory of the lattice thermal conductivity in diamond *Phys. Rev.* B **80** 125203

[40] de Koker N 2009 Thermal conductivity of MgO periclase from equilibrium first principles molecular dynamics *Phys. Rev. Lett.* **103** 125902

[41] Broido D A, Ward A and Mingo N 2005 Lattice thermal conductivity of silicon from empirical interatomic potentials *Phys. Rev.* B **72** 014308

[42] Yin M T and Cohen M L 1982 Theory of lattice-dynamical properties of solids: application to Si and Ge *Phys. Rev.* B **26** 3259–72

[43] Giannozzi P, de Gironcoli S, Pavone P and Baroni S 1991 *Ab initio* calculation of phonon dispersions in semiconductors *Phys. Rev.* B **43** 7231–42

[44] Baroni S, de Gironcoli S, Dal Corso A and Giannozzi P 2001 Phonons and related crystal properties from density-functional perturbation theory *Rev. Mod. Phys.* **73** 515–62

[45] Baroni S, Giannozzi P and Testa A 1987 Green's-function approach to linear response in solids *Phys. Rev. Lett.* **58** 1861–4

[46] Gonze X and Vigneron J-P 1989 Density-functional approach to nonlinear-response coefficients of solids *Phys. Rev.* B **39** 13120–8

[47] Debernardi A, Baroni S and Molinari E 1995 Anharmonic phonon lifetimes in semiconductors from density-functional perturbation theory *Phys. Rev. Lett.* **75** 1819–22

[48] Debernardi A 1998 Phonon linewidth in III-V semiconductors from density-functional perturbation theory *Phys. Rev.* B **57** 12847–58

[49] Deinzer G, Birner G and Strauch D 2003 *Ab initio* calculation of the linewidth of various phonon modes in germanium and silicon *Phys. Rev.* B **67** 144304

[50] Esfarjani K and Stokes H T 2008 Method to extract anharmonic force constants from first principles calculations *Phys. Rev.* B **77** 144112

[51] Ward A and Broido D A 2010 Intrinsic phonon relaxation times from first-principles studies of the thermal conductivities of si and ge *Phys. Rev.* B **81** 085205

[52] Li W, Lindsay L, Broido D A, Stewart D A and Mingo N 2012 Thermal conductivity of bulk and nanowire $Mg_2Si_xSn_x$ alloys from first principles *Phys. Rev.* B **86** 174307

[53] Broido D A, Lindsay L and Reinecke T L 2013 *Ab initio* study of the unusual thermal transport properties of boron arsenide and related materials *Phys. Rev.* B **88** 214303

[54] Lindsay L, Broido D A and Reinecke T L 2013 *Ab initio* thermal transport in compound semiconductors *Phys. Rev.* B **87** 165201

[55] Li W and Mingo N 2013 Thermal conductivity of bulk and nanowire InAs AlN and BeO polymorphs from first principles *J. Appl. Phys.* **114** 183505

[56] Esfarjani K, Chen G and Stokes H T 2011 Heat transport in silicon from first-principles calculations *Phys. Rev.* B **84** 085204

[57] Luo T, Garg J, Shiomi J, Esfarjani K and Chen G 2013 Gallium arsenide thermal conductivity and optical phonon relaxation times from first-principles calculations *Europhys. Lett.* **101** 16001

[58] Liao B, Lee S, Esfarjani K and Chen G 2014 First-principles study of thermal transport in FeSb2 *Phys. Rev.* B **89** 035108

[59] Wee D, Kozinsky B, Marzari N and Fornari M 2010 Effects of filling in CoSb_3: local structure, band gap, and phonons from first principles *Phys. Rev.* B **81** 045204

[60] Lindsay L, Broido D A and Reinecke T L 2013 Phonon-isotope scattering and thermal conductivity in materials with a large isotope effect: a first-principles study *Phys. Rev.* B **88** 144306

[61] Mingo N, Esfarjani K, Broido D A and Stewart D A 2010 Cluster scattering effects on phonon conduction in graphene *Phys. Rev.* B **81** 045408

[62] Lindsay L, Broido D A and Reinecke T L 2013 First-principles determination of ultrahigh thermal conductivity of boron arsenide: a competitor for diamond? *Phys. Rev. Lett.* **111** 025901

[63] Lindsay L, Broido D A and Reinecke T L 2012 Thermal conductivity and large isotope effect in GaN from first principles *Phys. Rev. Lett.* **109** 095901

[64] Stewart D A, Savić I and Mingo N 2009 First-principles calculation of the isotope effect on boron nitride nanotube thermal conductivity *Nano Lett.* **9** 81–4

[65] Li W, Mingo N, Lindsay L, Broido D A, Stewart D A and Katcho N A 2012 Thermal conductivity of diamond

nanowires from first principles *Phys. Rev.* B **85** 195436
[66] Mingo N, Stewart D A, Broido D A and Srivastava D 2008 Phonon transmission through defects in carbon nanotubes from first principles *Phys. Rev.* B **77** 033418
[67] Lindsay L, Broido D A and Mingo N 2009 Lattice thermal conductivity of single-walled carbon nanotubes: beyond the relaxation time approximation and phonon–phonon scattering selection rules *Phys. Rev.* B **80** 125407
[68] Broido D A, Lindsay L and Ward A 2012 Thermal conductivity of diamond under extreme pressure: a first-principles study *Phys. Rev.* B **86** 115203
[69] Shiomi J, Esfarjani K and Chen G 2011 Thermal conductivity of half-Heusler compounds from first-principles calculations *Phys. Rev.* B **84** 104302
[70] Shiga T, Shiomi J, Ma J, Delaire O, Radzynski T, Lusakowski A, Esfarjani K and Chen G 2012 Microscopic mechanism of low thermal conductivity in lead telluride *Phys. Rev.* B **85** 155203
[71] Tian Z, Garg J, Esfarjani K, Shiga T, Shiomi J and Chen G 2012 Phonon conduction in PbSe PbTe and $PbTe_1xSe_x$ from first-principles calculations *Phys. Rev.* B **85** 184303
[72] Murakami T, Shiga T, Hori T, Esfarjani K and Shiomi J 2013 Importance of local force fields on lattice thermal conductivity reduction in $PbTe_1xSe_x$ alloys *Europhys. Lett.* **102** 46002
[73] Lee S, Esfarjani K, Mendoza J, Dresselhaus M S and Chen G 2014 Lattice thermal conductivity of Bi, Sb, and Bi–Sb alloy from first principles *Phys. Rev.* B **89** 085206
[74] Lee S, Esfarjani K, Luo T, Zhou J, Tian Z and Chen G 2014 Resonant bonding leads to low lattice thermal conductivity *Nat. Commun.* **5** 3525
[75] Garg J, Bonini N, Kozinsky B and Marzari N 2011 Role of disorder and anharmonicity in the thermal conductivity of silicon–germanium alloys: a first-principles study *Phys. Rev. Lett.* **106** 045901
[76] Garg J and Chen G 2013 Minimum thermal conductivity in superlattices: a first-principles formalism *Phys. Rev.* B **87** 140302
[77] Garg J, Bonini N and Marzari N 2011 High thermal conductivity in short-period superlattices *Nano Lett.* **11** 5135–41
[78] Li W, Carrete J and Mingo N 2013 Thermal conductivity and phonon linewidths of monolayer MoS_2 from first principles *Appl. Phys. Lett.* **103** 253103
[79] Bonini N, Garg J and Marzari N 2012 Acoustic phonon lifetimes and thermal transport in free-standing and strained graphene *Nano Lett.* **12** 2673–8
[80] Paulatto L, Mauri F and Lazzeri M 2013 Anharmonic properties from a generalized third-order *ab initio* approach: theory and applications to graphite and graphene *Phys. Rev.* B **87** 214303
[81] Cuffe J *et al* 2014 Reconstructing phonon mean free path contributions to thermal conductivity using nanoscale membranes (arXiv:1408.6747)
[82] Henry A S and Chen G 2008 Spectral phonon transport properties of silicon based on molecular dynamics simulations and lattice dynamics *J. Comput. Theor. Nanosci.* **5** 141–52
[83] Tian Z, Esfarjani K, Shiomi J, Henry A S and Chen G 2011 On the importance of optical phonons to thermal conductivity in nanostructures *Appl. Phys. Lett.* **99** 053122
[84] Slack G A 1973 Nonmetallic crystals with high thermal conductivity *J. Phys. Chem. Solids* **34** 321–35
[85] Zhang W, Fisher T S and Mingo N 2007 The atomistic green's function method: an efficient simulation approach for nanoscale phonon transport *Numer. Heat Transfer Part B: Fundam.* **51** 333–49
[86] Chalopin Y, Esfarjani K, Henry A, Volz S and Chen G 2012 Thermal interface conductance in Si/Ge superlattices by equilibrium molecular dynamics *Phys. Rev.* B **85** 195302
[87] McGaughey A J H and Kaviany M 2006 Phonon transport in molecular dynamics simulations: formulation and thermal conductivity prediction *Advances in Heat Transfer* vol 39, ed G A Greene *et al* (New York: Academic) pp 169–255
[88] Landry E S and McGaughey A J H 2009 Thermal boundary resistance predictions from molecular dynamics simulations and theoretical calculations *Phys. Rev.* B **80** 165304
[89] Zuckerman N and Lukes J R 2008 Acoustic phonon scattering from particles embedded in an anisotropic medium: a molecular dynamics study *Phys. Rev.* B **77** 094302
[90] Schelling P K, Phillpot S R and Keblinski P 2002 Phonon wave-packet dynamics at semiconductor interfaces by molecular-dynamics simulation *Appl. Phys. Lett.* **80** 2484
[91] Datta S 2005 *Quantum Transport: Atom to Transistor* (Cambridge: Cambridge University Press)
[92] Datta S 1997 *Electronic Transport in Mesoscopic Systems* (Cambridge: Cambridge University Press)
[93] Datta S 2000 Nanoscale device modeling: the Green's function method *Superlatt. Microstruct.* **28** 253–78
[94] Mingo N 2009 Green's function methods for phonon transport through nano-contacts *Thermal Nanosystems and Nanomaterials* ed S Volz (*Topics in Applied Physics* vol 118) (Berlin: Springer) pp 63–94
[95] Mingo N and Yang L 2003 Phonon transport in nanowires coated with an amorphous material: an atomistic Green's function approach *Phys. Rev.* B **68** 245406
[96] Zhang W, Fisher T and Mingo N 2007 Simulation of interfacial phonon transport in Si–Ge heterostructures using an atomistic Green's function method *J. Heat Transfer* **129** 483
[97] Zhang W, Mingo N and Fisher T S 2007 Simulation of phonon transport across a non-polar nanowire junction using an atomistic Green's function method *Phys. Rev.* B **76** 195429
[98] Chalopin Y, Volz S and Mingo N 2009 Upper bound to the thermal conductivity of carbon nanotube pellets *J. Appl. Phys.* **105** 084301
[99] Kundu A, Mingo N, Broido D A and Stewart D A 2011 Role of light and heavy embedded nanoparticles on the thermal conductivity of SiGe alloys *Phys. Rev.* B **84** 125426
[100] Pernot G *et al* 2010 Precise control of thermal conductivity at the nanoscale through individual phonon-scattering barriers *Nat. Mater.* **9** 491–5
[101] Huang Z, Fisher T S and Murthy J Y 2010 Simulation of phonon transmission through graphene and graphene nanoribbons with a Green's function method *J. Appl. Phys.* **108** 094319
[102] Huang Z, Fisher T S and Murthy J Y 2010 Simulation of thermal conductance across dimensionally mismatched graphene interfaces *J. Appl. Phys.* **108** 114310
[103] Li X and Yang R 2012 Size-dependent phonon transmission across dissimilar material interfaces *J. Phys.: Condens. Matter* **24** 155302
[104] Li X and Yang R 2012 Effect of lattice mismatch on phonon transmission and interface thermal conductance across dissimilar material interfaces *Phys. Rev.* B **86** 054305
[105] Hopkins P E, Norris P M, Tsegaye M S and Ghosh A W 2009 Extracting phonon thermal conductance across atomic junctions: nonequilibrium Green's function approach compared to semiclassical methods *J. Appl. Phys.* **106** 063503
[106] Hopkins P E and Serrano J R Phonon localization and thermal rectification in asymmetric harmonic chains using a nonequilibrium Green's function formalism *Phys. Rev.* B **80** 201408

[107] Kim W, Zide J, Gossard A, Klenov D, Stemmer S, Shakouri A and Majumdar A 2006 Thermal conductivity reduction and thermoelectric figure of merit increase by embedding nanoparticles in crystalline semiconductors *Phys. Rev. Lett.* **96** 045901

[108] Majumdar A 1993 Microscale heat conduction in dielectric thin films *J. Heat Transfer* **115** 7–16

[109] Zhao H and Freund J B 2009 Phonon scattering at a rough interface between two fcc lattices *J. Appl. Phys.* **105** 013515

[110] Saltonstall C B, Polanco C A, Duda J C, Ghosh A W, Norris P M and Hopkins P E 2013 Effect of interface adhesion and impurity mass on phonon transport at atomic junctions *J. Appl. Phys.* **113** 013516

[111] Merabia S and Termentzidis K 2012 Thermal conductance at the interface between crystals using equilibrium and nonequilibrium molecular dynamics *Phys. Rev.* B **86** 094303

[112] Hyldgaard P and Mahan G D 1997 Phonon superlattice transport *Phys. Rev.* B **56** 10754–7

[113] Balasubramanian G and Puri I K 2011 Heat conduction across a solid-solid interface: understanding nanoscale interfacial effects on thermal resistance *Appl. Phys. Lett.* **99** 013116

[114] Landry E S and McGaughey A J H 2009 Effect of interfacial species mixing on phonon transport in semiconductor superlattices *Phys. Rev.* B **79** 075316

[115] Kiselev A A, Kim K W and Stroscio M A 2000 Thermal conductivity of si/ge superlattices: a realistic model with a diatomic unit cell *Phys. Rev.* B **62** 6896–9

[116] Tian Z, Esfarjani K and Chen G 2012 Enhancing phonon transmission across a Si/Ge interface by atomic roughness: first-principles study with the Green's function method *Phys. Rev.* B **86** 235304

[117] Chen P, Katcho N A, Feser J P, Li W, Glaser M, Schmidt O G, Cahill D G, Mingo N and Rastelli A 2013 Role of surface-segregation-driven intermixing on the thermal transport through planar Si/Ge superlattices *Phys. Rev. Lett.* **111** 115901

[118] Cheaito R, Duda J C, Beechem T E, Hattar K, Ihlefeld J F, Medlin D L, Rodriguez M A, Campion M J, Piekos E S and Hopkins P E 2012 Experimental investigation of size effects on the thermal conductivity of silicon-germanium alloy thin films *Phys. Rev. Lett.* **109** 195901

[119] Lee S-M, Cahill D G and Venkatasubramanian R 1997 Thermal conductivity of Si–Ge superlattices *Appl. Phys. Lett.* **70** 2957–9

[120] Huxtable S T, Abramson A R, Tien C-L, Majumdar A, LaBounty C, Fan X, Zeng G, Bowers J E, Shakouri A and Croke E T 2002 Thermal conductivity of si/SiGe and SiGe/SiGe superlattices *Appl. Phys. Lett.* **80** 1737–9

[121] Borca-Tasciuc T *et al* 2000 Thermal conductivity of symmetrically strained si/ge superlattices *Superlatt. Microstruct.* **28** 199–206

[122] Placzek G and Seidel W 1947 Milne's problem in transport theory *Phys. Rev.* **72** 550–5

[123] Mark C 1947 The neutron density near a plane surface *Phys. Rev.* **72** 558–64

[124] Hua C and Minnich A J 2014 Transport regimes in quasiballistic heat conduction *Phys. Rev.* B **89** 094302

[125] Collins K C, Maznev A A, Tian Z, Esfarjani K, Nelson K A and Chen G 2013 Non-diffusive relaxation of a transient thermal grating analyzed with the Boltzmann transport equation *J. Appl. Phys.* **114** 104302

[126] Joshi A A and Majumdar A 1993 Transient ballistic and diffusive phonon heat transport in thin films *J. Appl. Phys.* **74** 31–9

[127] Yang R, Chen G, Laroche M and Taur Y 2005 Simulation of nanoscale multidimensional transient heat conduction problems using ballistic-diffusive equations and phonon boltzmann equation *J. Heat Transfer* **127** 298–306

[128] Minnich A J, Chen G, Mansoor S and Yilbas B S 2011 Quasiballistic heat transfer studied using the frequency-dependent boltzmann transport equation *Phys. Rev.* B **84** 235207

[129] Rowlette J A and Goodson K E 2008 Fully coupled nonequilibrium electron–phonon transport in nanometer-scale silicon FETs *IEEE Trans. Electron Devices* **55** 220–32

[130] Sinha S, Pop E, Dutton R W and Goodson K E 2006 Non-equilibrium phonon distributions in sub-100 nm silicon transistors *J. Heat Transfer* **128** 638

[131] Sinha S and Goodson K E 2006 Thermal conduction in sub-100 nm transistors *Microelectron. J.* **37** 1148–57

[132] Klitsner T, VanCleve J E, Fischer H E and Pohl R O 1988 Phonon radiative heat transfer and surface scattering *Phys. Rev.* B **38** 7576–94

[133] Peterson R B 1994 Direct simulation of phonon-mediated heat transfer in a Debye crystal *J. Heat Transfer* **116** 815–22

[134] Lacroix D, Joulain K, Terris D and Lemonnier D 2006 Montductivity of silicon nanowires *Appl. Phys. Lett.* **89** 103104

[135] Mazumder S and Majumdar A 2001 Monte carlo study of phonon transport in solid thin films including dispersion and polarization *J. Heat Transfer* **123** 749–59

[136] Mittal A and Mazumder S 2010 Monte carlo study of phonon heat conduction in silicon thin films including contributions of optical phonons *J. Heat Transfer* **132** 052402

[137] Hao Q, Chen G and Jeng M-S 2009 Frequency-dependent monte carlo simulations of phonon transport in 2D porous silicon with aligned pores *J. Appl. Phys.* **106** 114321

[138] Jeng M-S, Yang R, Song D and Chen G 2008 Modeling the thermal conductivity and phonon transport in nanoparticle composites using monte carlo simulation *J. Heat Transfer* **130** 042410

[139] Narumanchi S V J, Murthy J Y and Amon C H 2003 Simulation of unsteady small heat source effects in sub-micron heat conduction *J. Heat Transfer* **125** 896–903

[140] Narumanchi S V J, Murthy J Y and Amon C H 2005 Comparison of different phonon transport models for predicting heat conduction in silicon-on-insulator transistors *J. Heat Transfer* **127** 713–23

[141] Narumanchi S V J, Murthy J Y and Amon C H 2004 Submicron heat transport model in silicon accounting for phonon dispersion and polarization *J. Heat Transfer* **126** 946–55

[142] McGaughey A J H and Jain A 2012 Nanostructure thermal conductivity prediction by Monte Carlo sampling of phonon free paths *Appl. Phys. Lett.* **100** 061911

[143] Heino P 2010 Lattice-boltzmann finite-difference model with optical phonons for nanoscale thermal conduction *Comput. Math. Appl.* **59** 2351–9 (*Mesoscopic Methods in Engineering and Science, Int. Conf. on Mesoscopic Methods in Engineering and Science (Edmonton, Canada, 12–16 July 2013)*)

[144] Péraud J-P M and Hadjiconstantinou N G 2012 An alternative approach to efficient simulation of micro/nanoscale phonon transport *Appl. Phys. Lett.* **101** 153114

[145] Radtke G A and Hadjiconstantinou N G 2009 Variance-reduced particle simulation of the Boltzmann transport equation in the relaxation-time approximation *Phys. Rev.* E **79** 056711

[146] Péraud J-P M and Hadjiconstantinou N G 2011 Efficient simulation of multidimensional phonon transport using energy-based variance-reduced Monte Carlo formulations *Phys. Rev.* B **84** 205331

[147] Hadjiconstantinou N G, Radtke G A and Baker L L 2010 On variance-reduced simulations of the Boltzmann transport equation for small-scale heat transfer applications *J. Heat Transfer* **132** 112401–8

[148] Homolle T M M and Hadjiconstantinou N G 2007 A low-variance deviational simulation Monte Carlo for the Boltzmann equation *J. Comput. Phys.* **226** 2341–58

[149] Baker L L and Hadjiconstantinou N G 2005 Variance reduction for Monte Carlo solutions of the Boltzmann equation *Phys. Fluids* **17** 051703

[150] Hadjiconstantinou N 2014 Monte carlo methods for solving the boltzmann transport equation *Ann. Rev. Heat Transfer* **17** 205–65

[151] Ravichandran N K and Minnich A J 2014 Coherent and incoherent thermal transport in nanomeshes *Phys. Rev.* B **89** 205432

[152] Hua C and Minnich A J 2014 Importance of frequency-dependent grain boundary scattering in nanocrystalline silicon and silicon-germanium thermoelectrics *Semicond. Sci. Technol.* **29** 124004

[153] Ding D, Chen X and Minnich A J 2014 Radial quasiballistic transport in time-domain thermoreflectance studied using Monte Carlo simulations *Appl. Phys. Lett.* **104** 143104

[154] Yu J-K, Mitrovic S, Tham D, Varghese J and Heath J R 2010 Reduction of thermal conductivity in phononic nanomesh structures *Nat. Nano* **5** 718–21

[155] Tang J, Wang H-T, Lee D H, Fardy M, Huo Z, Russell T P and Yang P 2010 Holey silicon as an efficient thermoelectric material *Nano Lett.* **10** 4279–83

[156] Dechaumphai E and Chen R 2012 Thermal transport in phononic crystals: the role of zone folding effect *J. Appl. Phys.* **111** 073508

[157] Zen N, Puurtinen T A, Isotalo T J, Chaudhuri S and Maasilta I J 2014 Engineering thermal conductance using a 2D phononic crystal *Nat. Commun.* **5** 3435

[158] Wang Z, Alaniz J E, Jang W, Garay J E and Dames C 2011 Thermal conductivity of nanocrystalline silicon: importance of grain size and frequency-dependent mean free paths *Nano Lett.* **11** 2206–13

[159] Brown S R, Kauzlarich S M, Gascoin F and Jeffrey Snyder G 2006 Yb14MnSb11: new high efficiency thermoelectric material for power generation *Chem. Mater.* **18** 1873–7

[160] Cochran W, Cowley R A, Dolling G and Elcombe M M 1966 The crystal dynamics of lead telluride *Proc. R. Soc. Lond.* A **293** 433–51

[161] Alperin H A, Pickart S J, Rhyne J J and Minkiewicz V J 1972 Softening of the transverse-optic mode in PbTe *Phys. Lett.* A **40** 295–6

[162] Squires G L 2012 *Introduction to the Theory of Thermal Neutron Scattering* (Cambridge: Cambridge University Press)

[163] Shirane G, Shapiro S M and Tranquada J M 2002 *Neutron Scattering with a Triple-Axis Spectrometer: Basic Techniques* (Cambridge: Cambridge University Press)

[164] Delaire O *et al* 2011 Giant anharmonic phonon scattering in PbTe *Nat. Mater.* **10** 614–9

[165] Li C W *et al* 2014 Phonon self-energy and origin of anomalous neutron scattering spectra in SnTe and PbTe thermoelectrics *Phys. Rev. Lett.* **112** 175501

[166] Minnich A J 2013 Thermal transport: naturally glassy crystals *Nat. Nanotechnol.* **8** 392–3

[167] Morelli D T, Jovovic V and Heremans J P 2008 Intrinsically minimal thermal conductivity in cubic I-V-VI_2 semiconductors *Phys. Rev. Lett.* **101** 035901

[168] Minnich A J, Johnson J A, Schmidt A J, Esfarjani K, Dresselhaus M S, Nelson K A and Chen G 2011 A thermal conductivity spectroscopy technique to measure phonon mean free paths *Phys. Rev. Lett.* **107** 095901

[169] Dames C and Chen G 2005 Thermal conductivity of nanostructured thermoelectric materials *CRC Thermoelectrics Handbook: Macro to Nano* ed D Rowe (Boca Raton, FL: CRC Press)

[170] Yang F and Dames C 2013 Mean free path spectra as a tool to understand thermal conductivity in bulk and nanostructures *Phys. Rev.* B **87** 035437

[171] Chen G 1996 Nonlocal and nonequilibrium heat conduction in the vicinity of nanoparticles *J. Heat Transfer* **118** 539–45

[172] Ju Y S and Goodson K E 1999 Phonon scattering in silicon films with thickness of order 100 nm *Appl. Phys. Lett.* **74** 3005–7

[173] Johnson J A, Maznev A A, Cuffe J, Eliason J K, Minnich A J, Kehoe T, Sotomayor Torres C M, Chen G and Nelson K A 2013 Direct measurement of room-temperature nondiffusive thermal transport over micron distances in a silicon membrane *Phys. Rev. Lett.* **110** 025901

[174] Simons S 1971 The application of high frequency thermal propagation data to the measurement of phonon relaxation times *J. Phys. C: Solid State Phys.* **4** 2089

[175] Koh Y K and Cahill D G 2007 Frequency dependence of the thermal conductivity of semiconductor alloys *Phys. Rev.* B **76** 075207

[176] Siemens M E, Li Q, Yang R, Nelson K A, Anderson E H, Murnane M M and Kapteyn H C 2009 Quasi-ballistic thermal transport from nanoscale interfaces observed using ultrafast coherent soft x-ray beams *Nat. Mater.* **9** 26–30

[177] Regner K T, Sellan D P, Su Z, Amon C H, McGaughey A J H and Malen J A 2013 Broadband phonon mean free path contributions to thermal conductivity measured using frequency domain thermoreflectance *Nat. Commun.* **4** 1640

[178] Freedman J P, Leach J H, Preble E A, Sitar Z, Davis R F and Malen J A 2013 Universal phonon mean free path spectra in crystalline semiconductors at high temperature *Sci. Rep.* **3** 2963

[179] Maznev A A, Nelson K A and Rogers J A 1998 Optical heterodyne detection of laser-induced gratings *Opt. Lett.* **23** 1319–21

[180] Johnson J A, Maznev A A, Bulsara M T, Fitzgerald E A, Harman T C, Calawa S, Vineis C J, Turner G and Nelson K A 2012 Phase-controlled, heterodyne laser-induced transient grating measurements of thermal transport properties in opaque material *J. Appl. Phys.* **111** 023503

[181] Minnich A J 2012 Determining phonon mean free paths from observations of quasiballistic thermal transport *Phys. Rev. Lett.* **109** 205901

[182] Maznev A A, Johnson J A and Nelson K A 2011 Onset of nondiffusive phonon transport in transient thermal grating decay *Phys. Rev.* B **84** 195206

[183] Grant M and Boyd S 2008 Graph implementations for nonsmooth convex programs *Recent Advances in Learning and Control* (*Lecture Notes in Control and Information Sciences*) ed V Blondel *et al* (New York: Springer) pp 95–110

[184] Grant M and Boyd S 2011 CVX: matlab software for disciplined convex programming, version 1.21 ../../cvx (http://cvxr.com/cvx)